



HAL
open science

A Non-isothermal model of a Laboratory Intermediate Temperature Fuel Cell using PBI doped Phosphoric Acid Membranes

Tiago Sousa, Mohamed Mamlouk, Keith Scott

► **To cite this version:**

Tiago Sousa, Mohamed Mamlouk, Keith Scott. A Non-isothermal model of a Laboratory Intermediate Temperature Fuel Cell using PBI doped Phosphoric Acid Membranes. *Fuel Cells*, 2010, 10 (6), pp.993. 10.1002/fuce.200900178 . hal-00574807

HAL Id: hal-00574807

<https://hal.science/hal-00574807>

Submitted on 9 Mar 2011

HAL is a multi-disciplinary open access archive for the deposit and dissemination of scientific research documents, whether they are published or not. The documents may come from teaching and research institutions in France or abroad, or from public or private research centers.

L'archive ouverte pluridisciplinaire **HAL**, est destinée au dépôt et à la diffusion de documents scientifiques de niveau recherche, publiés ou non, émanant des établissements d'enseignement et de recherche français ou étrangers, des laboratoires publics ou privés.



A Non-isothermal model of a Laboratory Intermediate Temperature Fuel Cell using PBI doped Phosphoric Acid Membranes

Journal:	<i>Fuel Cells</i>
Manuscript ID:	fuce.200900178.R1
Wiley - Manuscript type:	Original Research Paper
Date Submitted by the Author:	07-Apr-2010
Complete List of Authors:	Sousa, Tiago; Newcastle University, School of Chemical Engineering and Advanced Materials Mamlouk, Mohamed; Newcastle University, School of Chemical Engineering and Advanced Materials Scott, Keith; Newcastle University, School of Chemical Engineering and Advanced Materials
Keywords:	Numerical Simulation, PEMFC Model, Intermediate Temperature Fuel Cell, Non-isothermal, Polybenzimidazole



A Non-isothermal model of a Laboratory Intermediate Temperature Fuel Cell using PBI doped Phosphoric Acid Membranes

T. Sousa, M. Mamlouk and K. Scott*

*School of Chemical Engineering and Advanced Materials,
Newcastle University, NE1 7RU, UK*

**Corresponding author, k.scott@ncl.ac.uk*

Keywords. Polybenzimidazole; Numerical Simulation; Intermediate Temperature Fuel Cell; PEMFC Model; Non-isothermal

Abstract

A two-dimensional non-isothermal model developed for a single Intermediate Temperature Fuel Cell with a phosphoric acid doped PBI membrane is developed. The model of the experimental cell incorporates the external heaters, and the all body of the fuel cell. The catalyst layers were treated as spherical catalyst particles agglomerates with porous inter-agglomerate space. The inter-agglomerate space is filled with a mixture of electrolyte (hot phosphoric acid) and PTFE. All the major transport phenomena are taken into account except the crossover of species through the membrane. This model was used to study the influence of two different geometries (along the channel direction and cross the channel direction) on performance. It became clear, through the performance analyses, that the predictions obtained by the along the channel geometry did not represent the general performance trend, and therefore this geometry is not appropriate for fuel cell simulations. Results also indicate that the catalyst layer was not efficiently used, which leads to large temperatures differences through the MEA.

1 Introduction

Conventional PEMFCs have typically used Nafion[®] or similar perfluorinated polymer as membrane. The proton conductivity of these membranes strongly depends on its water content. This feature leads to temperature restrictions during fuel cell operation, i.e. it can only operate efficiently below the water boiling point, otherwise the membrane dehydrates and its conductivity falls drastically. In order to maintain the correct water balance the inlet streams must be humidified. As a consequence of the low operating temperature (typically 80 °C), fuel cells with Nafion[®] membranes exhibit three main problems: inadequate water and heat management, sluggish electrochemical kinetics, and intolerance to impurities, mainly carbon monoxide (CO). To overcome these problems much effort has been made to develop polymer membranes capable of retaining high proton conductivity at higher temperatures without humidification. Poly[2,2-(m-phenylene)-5,5 bibenzimidazole doped with phosphoric acid, generically referred to as polybenzimidazole (PBI), is one membrane that has been proposed in recent years. This kind of membrane has been considered as a promising candidate for use in intermediate temperature PEMFCs [1-5], as although other kinds of polymer and hybrid membranes are under intensive research [6-17].

Modelling plays an important role in fuel cell technology because it increases understanding of its behaviour, enables prediction of its performance, and assists with its operational control. Bernardi and Verbrugge [18] were the first to develop a model for a PEMFC running with a Nafion[®] membrane. This model was one-dimensional (1D), isothermal and for steady state conditions. It was applied only at the oxygen electrode in order to study the polarization characteristics, water transport, and catalyst utilization. A significant amount of work has been produced since this first model and reviews of the subject have been made [19-21].

In comparison with Nafion[®] based PEMFCs, only a few publications have considered models for PBI based PEMFCs. Korsgaard et al. [22] developed a simple semi-empirical model to correlate their experimental data. The model showed good agreement with the experimental data, although only predicted the polarisation curves based on the cathode activation overpotential, ohmic and concentration losses. Cheddie and Munroe, [23-26] developed several papers on this particular issue. In all of them, heat generation due to the electrochemical reaction, and ohmic heating were taken into account. The most recent work [26] was an improvement of the previous models, which accounted for two phase effects due to the transport of dissolved species in phosphoric acid/PBI catalyst layer, and considered aqueous phase electrochemical reactions. This model showed a good fit with the

Field Code Changed

1 experimental data and suggested that transport limitations were significant at both electrodes.
2 It also predicted that the catalyst layers effective utilization was very low, between 0.1% and
3 1%. More recent Scott et al. [27] developed a 1D model to simulate the effect of catalyst
4 loading and the Pt/carbon ratio on cell performance. Field Code Changed

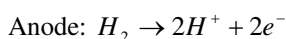
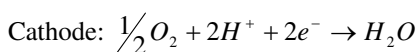
5
6 This current paper reports the results of a two dimensional (2D) non-isothermal model
7 developed for a single intermediate temperature PEMFC with a phosphoric acid (PA) doped
8 PBI membrane and compares the simulation with laboratory cell data. The catalyst layer was
9 treated as catalyst particles agglomerates with porous inter-agglomerate spaces. The inter-
10 agglomerate spaces can be filled with a mixture of electrolyte, reactants and products.
11 Different agglomerate geometries can be adopted, however Broka and Ekdunge [28]
12 suggested that the spherical agglomerate is the appropriate choice to describe the catalyst
13 layer. Field Code Changed

21 2 Model

25 2.1 Physical Description and Assumptions

26
27 This work develops a 2D non-isothermal model for a single intermediate temperature
28 PEMFC with a phosphoric acid doped PBI membrane. The cell consists of the membrane
29 with bonded anode and cathodes catalyst layers which are covered by gas diffusion layers.
30
31

32
33 Oxygen and hydrogen (not humidified) were supplied to the cathode and anode,
34 respectively. The reactions in the cell were:
35
36



41
42
43 The methods and materials used in experimental tests can be found in [27, 29]. In brief the
44 fuel cell used in this study (shown schematically in [29]) consisted of a titanium cell body
45 with a 3 cm x 3 cm gold plated parallel flow fields. Mica filled PTFE inserts were used to
46 surround the flow fields and provide location for the O-ring seal and a dynamic hydrogen
47 reference electrode (DHE). The solid state DHE consisted of two platinum wires on each side
48 of the membrane located outside the O-ring: a distance of 10 mm away from the MEA edge
49
50
51
52

Deleted: [27]

Field Code Changed

Deleted:

Deleted: Figure 1

1 to avoid side current effects (the membrane used was $\sim 40\mu\text{m}$ thick). A small current $\sim 10\mu\text{A}$
2 (1.0 mA cm⁻²) was applied by means of 9.0 V battery connected in series with an appropriate
3 resistance.
4

5
6 The temperature of the cell was controlled by thermostatically controlled tubular heaters
7 inserted into the cell bodies. The relative humidity was obtained from an intrinsically safe
8 humidity sensor (Vaisala HUMICAP[®], Finland).
9

10 The membranes were prepared from PBI powder dissolved in N,N-dimethylacetamide
11 (DMAc) by casting onto optical glass and kept in an oven at a temperature of 90 to 110 °C
12 overnight to produce a 40 μm thick membrane. The catalyst ink was prepared either by
13 sonicating the catalyst and PBI in acetone/DMAc, for PBI based MEAs, or the catalyst and
14 PTFE dispersion (60%wt, Aldrich) in water-ethanol mixture, for PTFE based MEAs. Gas
15 diffusion electrodes (carbon cloth) incorporated with wet proofed micro porous layer (H2315
16 T10AC1) obtained from Freudenberg (FFCCT, Germany) were used as substrates to deposit
17 the catalyst layer for both anode and cathode. Anodes were prepared using 0.2 mg_{Pt} cm⁻² 20%
18 Pt/C (E TEK) with PBI loading of 0.28 and 0.7 mg cm⁻² and fixed doping level of 8 PRU.
19 MEAs were prepared by hot pressing the GDL supported catalysts onto the PBI membrane at
20 150 °C and 40 kg cm⁻² for 10 min.
21

22 For the fuel cell simulations we were particular interested in analysing the effect of
23 different computational domains on model predictions. Therefore, two different
24

25 computational domains were employed for the simulations (Geometry A and Geometry B).

26 As can be seen in Figure 1, Geometry A consisted of a yz-plane which took into account the
27 complete fuel cell body (including: titanium body, PTEF isolation layer, heaters, gas
28 channels and MEA). With this computational domain it was possible to analyse variations
29 along-the-channel (y) and through the membrane (z) due to changes in concentration and
30 pressure. Figure 2 shows details of this computational domain, where it is possible to see
31 with this geometry only two gas channels were modelled, one in the anode side and another
32 in cathode side.

33
34
35
36
37
38
39
40
41
42
43
44
45
46
47
48
49
50
51
52
53
54
55
56
57
58
59
60
Geometry B, also took into account the entire fuel cell body but in a different direction (in
this case the xz orientation, as Figure 3 shows). Therefore, this computational domain models
an array of channels and considered variations across-the-channel (x) and through the
membrane (z) which made possible the analysis of the effect of ribs on performance. With
this computational domain 24 channels were modelled (12 in the cathode side and another 12
in the anode side) and the effect of 26 ribs could be analysed.

Deleted: geometries

Deleted: Geometry A considered variations along-the-channel and through the membrane

Deleted: in

Deleted: all

Deleted: x

Deleted: of

Deleted: drops

Deleted: a

Deleted: as

Deleted: it was used

Deleted:

Deleted: z

Deleted: x

For both computational domains, the MEA was divided into 7 different sub-domains: anode and cathode gas diffusion layers (GDL), anode and cathode micro-porous layers (MPL), anode and cathode catalyst layers and the membrane. All the relevant geometric parameters and operational properties are shown in Table 1.

Deleted: The intersection of both geometries is a line parallel to the z-axis exactly in the centre of the cell. Geometry A is especially useful to analyse changes along the channel due to changes of concentration and pressure drops, on the other hand, Geometry B will be focus in the effect of the ribs between channels.¶
Several sub-domains were defined within both geometries in order to successfully implement the numeric solution of the various equations. As can be seen in Figure 2, f

Deleted: geometries

In this model a number of assumptions were adopted:

- (i) Steady state operation.
- (ii) Single phase flow.
- (iii) Ideal gas mixtures.
- (iv) Porous media was assumed to be isotropic and macro-homogeneous.
- (v) The PBI membrane was assumed to be impermeable to gas flow.
- (vi) Negligible contact resistance between components.
- (vii) Heat transfer through radiation was neglected.

2.2 Governing Equations

This section provides the governing equations which describe the physical, chemical, electrical and electrochemical processes occurring in the PEMFC described above.

Deleted: ¶

2.2.1 Conservation of Momentum

At the gas channels, the gas flow field and pressure was obtained by solving the equation of continuity (Eq. (1)) and the weakly compressible form of the Navier Stokes equation (Eq. (2)).

$$\nabla \cdot (\rho \mathbf{v}) = 0 \quad (1)$$

$$\rho \mathbf{v} \cdot \nabla \mathbf{v} = -\nabla p + \nabla \cdot (\mu \Gamma) \quad (2)$$

Where, ρ is the density, \mathbf{v} is the velocity vector, p is the fluid pressure, μ is the fluid viscosity and Γ is the deviatoric strain-rate, which is defined by:

$$\Gamma = \nabla \mathbf{v} + (\nabla \mathbf{v})^T - \frac{2}{3}(\nabla \cdot \mathbf{v}) \quad (3)$$

In the porous media Eq. (2) had to be corrected for porosity. Therefore, Brinkman's equation (which is a generalization of Darcy's law that facilitates the matching of boundary conditions between porous media and free media [30]) was used [31]:

Deleted: the Navier Stokes equation

Field Code Changed

Field Code Changed

$$\mathbf{v} \frac{\mu^{eff}}{K} = -\nabla p + \nabla \cdot \left(\frac{\mu^{eff}}{\varepsilon} \Gamma \right) \quad (4)$$

Where, K is the permeability of the porous media, ε is the porosity of the porous media, and μ^{eff} is the effective viscosity

2.2.2 Conservation of Species

The mass conservation for the individual gas phase species was obtained by solving the Stefan-Maxwell equations [27]:

$$\nabla \cdot \left[\rho w_i \sum_j \tilde{D}_{ij}^{eff} \left(\nabla x_j + \left(x_j - x_j \frac{M_j}{\bar{M}} \right) \frac{\nabla p}{p} \right) \right] - \rho \mathbf{v} \nabla \cdot w_i + St_s = 0 \quad (5)$$

In Eq. (5), w_i is the mass fraction of the species i , x_j is the mole fraction of species j , M_j is the molecular weight of species j , \bar{M} is the average molecular weight, St_s is the source term for the conservation of species, and \tilde{D}_{ij}^{eff} is the effective binary diffusivity of the pair i, j .

The source term accounts for the local rates of oxygen and hydrogen consumption and water vapour production. Therefore, the source term only assumes a value different to zero in the catalyst layers, because the electrochemical reactions only occur in these layers.

$$St_{s,H_2} = j_a \frac{M_{H_2}}{2F} \quad (6)$$

$$St_{s,O_2} = -j_c \frac{M_{O_2}}{4F} \quad (7)$$

$$St_{s,H_2O} = j_c \frac{M_{H_2O}}{2F} \quad (8)$$

Where j_a is the anode volumetric current density, j_c is the cathode volumetric current density, M is the molecular weight for the different species, and F is the Faraday constant.

Deleted:

Deleted: [25]

Deleted: n_i is the mass fraction vector of the species i .

2.2.3 Conservation of Charge

The transport of current was obtained by solving Ohm's law for both electrical and electronic current.

$$\nabla \cdot (-k_s^{eff} \nabla \phi_s) = St_{\phi_s} \quad (9)$$

$$\nabla \cdot (-k_{elect}^{eff} \nabla \phi_{elect}) = -St_{\phi_{elect}} \quad (10)$$

Where, k_s^{eff} is the effective electrical conductivity in the porous media, k_{elect}^{eff} is the effective electrolyte conductivity in the porous media, ϕ_s is the solid phase potential, ϕ_{elect} is the electrolyte phase potential, St_{ϕ_s} and $St_{\phi_{elect}}$ are the source terms representing the volumetric transfer current for the solid phase, and the electrolyte phases respectively.

2.2.4 Kinetics and Thermodynamics

The Butler-Volmer equation was used to describe the kinetics at the anode and cathode.

$$j = a_{pt} i_0 \left[\exp\left(\frac{-\alpha_{rd} F}{RT} \eta\right) - \exp\left(\frac{\alpha_{ox} F}{RT} \eta\right) \right] \quad (11)$$

Where, a_{pt} is the electrocatalytic surface area, α is the transfer coefficient, R is the universal gas constant, T is the temperature, i_0 is the exchange current density which is corrected for the particular conditions of pressure and temperature of the system., and η is the overpotential.

The catalyst layers were treated as spherical agglomerates of catalyst particles with porous inter-agglomerate space, where each agglomerate is covered by a thin film of electrolyte. Therefore, Eq. (11) was modified to account for the geometry of the agglomerate and the transport of the dissolved species through it.

$$j = nFC_{ig/l} \left[\frac{1}{Er k_c (1 - \varepsilon_{CAT})} + \frac{(r_{agg} + \delta)\delta}{r_{agg} a_{agg} D_{liq,i}} \right]^{-1} \quad (12)$$

Where, k_c is the reaction rate constant, $C_{ig/l}$ is the concentration of the reactants at the gas/liquid interface, Er is the effectiveness factor, a_{agg} is the effective agglomerate surface area, r_{agg} is the agglomerate radius, $D_{liq,i}$ is the reactants diffusion in phosphoric acid, δ is the thin film thickness.

The reaction rate was obtained by the following equation:

$$k_c = \frac{i_0}{nF(1 - \varepsilon_{CAT})C_{il/s}} \left[\exp\left(\frac{-\alpha_{Rd}F}{RT}\eta\right) - \exp\left(\frac{\alpha_{Ox}F}{RT}\eta\right) \right] \quad (13)$$

A detailed explanation about the above approach is given in Appendix A

The overpotential, η , is the electrochemical reaction driving force and is defined by the potential difference between the solid and electrolyte phase :

$$\eta = \phi_s - \phi_m - V_{ref} \quad (14)$$

The reference potential, V_{ref} , on the anode side is zero and is equal to the theoretical cell potential at a given temperature and pressure on the cathode given by Nernst equation.

$$V_{ref} = -\left(\frac{\Delta H}{nF} - \frac{T\Delta S}{nF}\right) + \frac{RT}{nF} \ln \left[\frac{(RT)^{1.5} C_{H_2} C_{O_2}^{0.5}}{a_{H_2O}} \right] \quad (15)$$

Where, ΔH is the enthalpy change, ΔS is the entropy change, C_{H_2} is the hydrogen concentration (solubility) obtained using Henry's law, C_{O_2} is the oxygen concentration (solubility) obtained using Henry's law, and, a_{H_2O} is the water activity.

2.2.5 Conservation of Energy

The conservation of energy for any sub-domain was described as follows:

$$\nabla \cdot (-k_T \nabla T) = \rho c_p \mathbf{v} \cdot \nabla T + S_e \quad (16)$$

Where, k_T is the thermal conductivity, c_p is the species heat capacity, and S_e is the energy source term.

The energy equation accounted for conduction, convection and heat generation due to Joule heating, as well as the heat of reaction. Joule heating, q_{Joule} , was taken into account in the GDLs, MPL, catalyst layers, and membrane. In the collector plates Joule heating was assumed to be insignificant due to their high conductivity:

$$q_{Joule} = \phi^2 k \quad (17)$$

The fuel cell electrochemical reactions are exothermic and heat is generated during the fuel cell operation time. This heat generation is due to entropy changes and irreversibilities

caused by activation overpotential. An exhaustive study about this issue was presented in [32]. The heat of reaction, $q_{reaction}$ was calculated from:

$$q_{reaction} = \left(\frac{T\Delta S}{nF} - |\eta| \right) |j_c| \quad (18)$$

The heat of reaction is directly proportional to the entropy changes and overpotential. Because both of these contributions are very small at the anode side it was assumed that the heat of reaction was negligible at the anode side. It is well known that the overpotential at the anode side is very small compared to that at the cathode. From the data provided by Lampinen and Fomino [32] the half cell entropy change at the anode side and at the cathode side at 298.15 K were calculated as:

Entropy change at the anode side: $-0.104 \text{ J mol}^{-1} \text{ K}^{-1}$

Entropy change at the cathode side: $-44.3 \text{ J mol}^{-1} \text{ K}^{-1}$

Thus the entropy change at the anode side can be ignored when compared to the entropy change at the cathode side.

2.3 Boundary Conditions

In order to solve the governing equations, boundary conditions were applied for all variables of interest. As mentioned before this model was used in two different geometries; this fact leads to different boundary conditions for each geometry.

2.3.1 Geometry A

Momentum balance

The inlet velocity was set for both the anode and cathode sides. The inlet velocity used in the experimental work carried out in our laboratories was 0.1768 m s^{-1} and 0.0589 m s^{-1} for the cathode and anode, respectively. From these values the inlet velocities for each channel could be estimated.

Field Code Changed

Field Code Changed

Deleted: for

$$\mathbf{v} = \begin{cases} v_x = v_0^a \\ v_y = 0 \end{cases} \quad (19)$$

$$\mathbf{v} = \begin{cases} v_x = -v_0^c \\ v_y = 0 \end{cases} \quad (20)$$

Where, v_0^a is the anode inlet velocity and v_0^c is the cathode inlet velocity.

In the gas channels, outlets pressure was set for both anode and cathode as follows:

$$p = p_0 \quad (21)$$

Where p_0 is operational pressure.

Species balance

The inlet mass fraction was set for both the anode and cathode sides. At the anode non humidified hydrogen was used and air was fed to the cathode.

$$w_{H_2} = 1 \quad (22)$$

$$w_{O_2} = 0.23 \wedge w_{H_2O} = 0.011 \quad (23)$$

At the gas channels outlets, the convective flux sets the boundary condition:

$$n_{H_2} = w_{H_2} \rho \mathbf{v} \cdot \mathbf{n} \quad (24)$$

$$n_{O_2} = w_{O_2} \rho \mathbf{v} \cdot \mathbf{n} \wedge n_{H_2O} = w_{H_2O} \rho \mathbf{v} \cdot \mathbf{n} \quad (25)$$

Energy balance

In the experimental apparatus there was no thermocouple to measure the temperature of the gas feed at the gas channel inlets. As a consequence the inlet temperature was assumed to be equal to the fuel cell operating temperature.

$$T = T_0 \quad (26)$$

Where, T_0 is the operational temperature.

At the outlets a convective flux as boundary condition was applied.

$$\mathbf{n}(-k_T \nabla T) = 0 \quad (27)$$

At the exterior boundaries of the domain it was simply required to solve the conservation of energy, therefore, there we only required boundary conditions for this equation. It was assumed that a uniform surface heat flux existed for all exterior walls of the cell. It was also assumed that all exterior walls were subjected to the same exterior air velocity and temperature. To calculate the heat flux, q_{conv} , the following equation was used:

$$q_{conv} = \bar{h}(T - T_{air}) \quad (28)$$

Where, \bar{h} was the average heat transfer coefficient, and T_{air} was the average temperature of the exterior air.

The average heat transfer coefficient was calculated by the following equation:

$$\bar{h} = \frac{\bar{Nu} k_{T_{air}}}{L} \quad (29)$$

Where, \bar{Nu} is the average Nusselt number, $k_{T_{air}}$ is the thermal conductivity of the external air, L is the characteristic length.

The Nusselt number is a dimensionless parameter which accounts for the ratio of convective and conductive heat transfer through the boundary. For Reynolds numbers between 5×10^3 and 5×10^5 , with a uniform surface heat flux, and assuming that the fuel cell can be represented by a rectangular section it can be calculated as follows [33]:

$$\bar{Nu} = 0.102 \text{Re}^{0.675} \text{Pr}^{1/3} \quad (30)$$

Where, Re and Pr are the Reynolds and Prandtl numbers, respectively.

To simulate the heaters the temperature at the heaters/collector plate boundaries were prescribed to the desired operating temperature.

Charge balance

For the conservation of charge it was necessary to set boundary conditions for both solid and electrolyte phase potentials. The solid phase potential was prescribed at the rib/GDL interface. For the anode side it was set to zero volts, and to the cell potential at the cathode rib/GDL interface.

Field Code Changed

$$\phi_s = 0 \text{ at the anode side} \quad (31)$$

$$\phi_s = V_{Cell} \text{ at the cathode side} \quad (32)$$

Where, V_{Cell} is the operational potential of the fuel cell.

For the electrolyte phase the potential was only required to prescribe electrical insulation to the exterior boundaries formed by the membrane and catalyst layers.

2.3.2 Geometry B

The boundary conditions for charge and energy balances were the same of Geometry A; however, there were major differences for momentum and species balance. From Fig. 3 it is possible to see that Geometry B did not include the gas channel inlets or outlets, therefore a different approach was applied to solve the momentum and species balance. It was assumed that the species were transported only through diffusion in the z and y directions, so the momentum balance was no longer needed. The species mass fraction was prescribed at the most interior wall of the gas channels. In order to increase the model accuracy these mass fractions should vary with potential. Figure 4 shows the variation of the average species mass fraction with potential at the gas channel/collector plate interface (these data was obtained with a 2D isothermal, along the channel model developed previously and described in [34]). These data were used to generate a set of equations which were utilized to predict the variation of the species mass fraction with potential.

$$w_{H_2} = \begin{cases} 1.12V_{Cell}^3 - 2.91V_{Cell}^2 + 2.52V_{Cell} + 0.274, & V_{Cell} \geq 0.7 \text{ V} \\ -0.6.97V_{Cell}^3 + 1.01V_{Cell}^2 - 6.57V_{Cell} + 0.798, & V_{Cell} < 0.7 \text{ V} \end{cases} \quad (33)$$

$$w_{O_2} = \begin{cases} 0.188V_{Cell}^3 - 0.482V_{Cell}^2 + 0.420V_{Cell} + 0.274, & V_{Cell} \geq 0.7 \text{ V} \\ -0.195V_{Cell}^3 + 0.230V_{Cell}^2 + 8.28 \times 10^{-4} V_{Cell} + 0.184, & V_{Cell} < 0.7 \text{ V} \end{cases} \quad (34)$$

$$w_{H_2O} = \begin{cases} -0.216V_{Cell}^3 + 0.560V_{Cell}^2 - 0.483V_{Cell} + 0.150, & V_{Cell} \geq 0.7 \text{ V} \\ 0.224V_{Cell}^3 - 0.264V_{Cell}^2 - 7.46 \times 10^{-4} V_{Cell} + 6.35 \times 10^{-2}, & V_{Cell} < 0.7 \text{ V} \end{cases} \quad (35)$$

Deleted: ure

Deleted: 2 - B

Deleted: 3

2.4 Constitutive Relations and Model Parameters

Most of the materials and species properties were treated as variables which depended on temperature, pressure and concentration. The relationship between these properties and the dependent variables are well documented in the literature; therefore this issue will not be subject of attention in this paper. Table 2 show the key parameters that were used for the simulations.

The species transport through the agglomerates was extremely important in this system. The diffusion of gases through liquid media had a big impact on performance; in particular at high current densities due to the relative low diffusion coefficient. At high current densities the reaction rate was mainly limited by the sluggish transport of oxygen in the catalyst layer.

Both the Henry's constant and diffusion coefficient for oxygen in phosphoric acid depend on temperature and phosphoric acid concentration. From the experimental data provided by Klinedinst et al. [35], a function to calculate the Henry's constant, H_{O_2} , and diffusion coefficient, D_{liqO_2} , for oxygen in hot phosphoric acid was built:

$$H_{O_2} = \exp\left(\left(-1.27 \times 10^4 w_{H_3PO_4} + 1.23 \times 10^4\right) \frac{1}{T} + (35.2 w_{H_3PO_4} - 46.6)\right) \quad (36)$$

$$D_{liqO_2} = \exp\left(\begin{aligned} &\left(-9.21 \times 10^5 w_{H_3PO_4}^3 + 2.47 \times 10^6 w_{H_3PO_4}^2 - 2.21 \times 10^6 w_{H_3PO_4} + 6.54 \times 10^5\right) \frac{1}{T} \\ &+ \left(1.66 \times 10^3 w_{H_3PO_4}^3 - 4.46 \times 10^3 w_{H_3PO_4}^2 + 4.01 \times 10^3 w_{H_3PO_4} + 1.21 \times 10^3\right) \end{aligned}\right) \quad (37)$$

Where, $w_{H_3PO_4}$ is the phosphoric acid mass fraction, which was calculated by the following equation [36]:

$$w_{H_3PO_4} = \frac{0.0544 x_{H_3PO_4}}{x_{H_3PO_4} (0.0544 - 0.01) + 0.01} \quad (38)$$

Where, $x_{H_3PO_4}$ is the phosphoric acid mole fraction.

To calculate the phosphoric acid mole fraction we assumed that the concentration of phosphoric acid remained constant and the local acid partial pressure was in equilibrium with the acid inside the agglomerate. Therefore, from the experimental data provided by [36] it was possible to generate a set of equations which coupled the concentration of phosphoric acid with the water partial pressure.

Deleted: [34]

Field Code Changed

Deleted: [35]

Field Code Changed

Field Code Changed

Deleted: [35]

$$x_{H_3PO_4} = \frac{\ln(p_{H_2O}) + \frac{2765.1}{T} - 22.002}{\frac{-4121.9}{T} + 2.5929} \quad (39)$$

Where, p_{H_2O} is the water partial pressure.

Due to insufficient experimental data, Eqs. (38)-(39) are only valid until 96 wt.% H_3PO_4 . Therefore, for concentrations higher than 96% the concentration term was kept constant and equal to 0.96.

As result of insufficient studies on hydrogen solubility and diffusion in hot phosphoric acid, the diffusion coefficient and Henry's constant cannot be correlated to experimental data. Thus, it was assumed that these parameters behave in the same way as in water systems [26]:

$$H_{H_2} = 4H_{O_2} \quad (40)$$

$$D_{liqH_2} = 2D_{liqO_2} \quad (41)$$

Where, H_{H_2} is the Henry's constant of hydrogen in phosphoric acid and D_{liqH_2} is the diffusion coefficient of hydrogen in phosphoric acid.

The proton conductivity has a big impact on fuel cell performance, particularly in intermediate temperatures PEM fuel cells, due to the relative low membrane conductivity. Bouchet and Siebert [37], and Ma et al. [38], proposed that the conductivity of PBI membranes doped with phosphoric acid obeyed an Arrhenius law:

$$\kappa_m = \frac{B}{T} \exp\left(-\frac{E_M}{RT}\right) \quad (42)$$

Where, B is the pre-exponential coefficient and E_M is the activation energy.

From the experimental data provided by Scott et al. [27] for a doping level of 5.6 mol of H_3PO_4 per PBI repeat unit, it was possible to generate two functions that correlated these two parameters with the relative humidity at a constant doping level.

$$E_M = (174.86RH + 698.47)R \quad (43)$$

$$B = \exp(0.5677RH + 8.6535) \quad (44)$$

In the catalyst layers the phosphoric acid that comes from the membrane was responsible for its proton conductivity. To calculate the conductivity of phosphoric acid the experimental data was fitted to a polynomial function [36]. The effective conductivity was obtained by the Bruggman model:

Field Code Changed

Field Code Changed

Deleted: [36]

Field Code Changed

Deleted: [37]

Field Code Changed

Deleted: [35]

Field Code Changed

$$k_{elect}^{eff} = k_{H_3PO_4} \varepsilon_{H_3PO_4}^{1.5} \quad (45)$$

Where, $k_{H_3PO_4}$ is the proton conductivity of phosphoric acid, and $\varepsilon_{H_3PO_4}$ is the fraction of phosphoric acid in the catalyst layer.

Isotropic conductivity for all regions where the transport of electrons occurs was assumed. This means that the model does not distinguish between in- and through plane conductivities. For the GDL the value reported by the supplier for the through plane conductivity, 1250 S/m was used [39]. At the MPL and catalyst layer the electron conductivity was calculated by taking into account the volume fraction of the materials responsible for the conductivity. The effective electron conductivity was obtained by the following equation [40]:

$$k_s^{eff} = k_s \frac{2 - 2\varepsilon_e}{\varepsilon_e + 2} \quad (46)$$

Formatted Table

Formatted: Indent: Before: 1.7 pt, First line: 0 pt, After: -1.95 pt

Where, k_s is the electrical conductivity of the solid phase (carbon black in the MPL and both platinum and carbon black in the catalyst layer), ε_e is the volume fraction of the non-conductor materials.

The electrical conductivity of Vulcan XC-72 carbon black was reported by Pantea et al. [41] to be equal to 450 S m⁻¹. The electrical conductivity of platinum, k_{Pt} , was obtained from the data provided by Powel and Tye [42]. From these data a linear function was generated to correlate the electrical conductivity of platinum $\ln(k_s)$ with temperature $\ln(T)$:

$$\ln(k_{Pt}) = -0.93 \ln(T) + 21.3 \quad (47)$$

Formatted Table

Formatted: Indent: First line: 0 pt, After: 1.7 pt, Tabs: 50.85 pt, Left

The electric conductivity of the titanium flow fields and carbon paper was assumed constant with temperature and equal to 1.92 x 10⁶ S m⁻¹ [43] and 1250 S m⁻¹ [44], respectively.

The thermal conductivity of the gas mixture $k_{T,fluid}$ was obtained from a semiempirical equation developed by Wilke in 1950 [45]:

$$k_{T,fluid} = \frac{\sum_{i=1}^n x_i k_{T,i}}{\sum_{j=1}^n x_j \Phi_{ij}} \quad (48)$$

Formatted Table

In which:

$$\Phi_{ij} = \frac{1}{\sqrt{8}} \left(1 + \frac{M_i}{M_j} \right)^{-1/2} \left[1 + \left(\frac{k_{T,i}}{k_{T,j}} \right)^{1/2} \left(\frac{M_j}{M_i} \right)^{1/4} \right]^2 \quad (49)$$

$$\Phi_{ji} = \frac{k_{T,j} M_i}{k_{T,i} M_j} \Phi_{ij} \quad (50)$$

$k_{T,i}$ is the thermal conductivity of the species and it was obtained for each species through

a linear regression of experimental data [46]:

$$k_{T,O_2} = 6.204 \times 10^{-5} T + 8.830 \times 10^{-3} \quad R^2 = 0.998 \quad (51)$$

$$k_{T,H_2} = 3.777 \times 10^{-4} T + 7.444 \times 10^{-2} \quad R^2 = 0.999 \quad (52)$$

$$k_{T,N_2} = 5.453 \times 10^{-5} T + 1.088 \times 10^{-2} \quad R^2 = 0.998 \quad (53)$$

$$k_{T,H_2O} = 1.189 \times 10^{-4} T + 2.32 \times 10^{-2} \quad R^2 = 0.996 \quad (54)$$

For platinum, carbon back, and PTFE the thermal conductivity was also obtained from a polynomial function. In the case of PTFE a linear equation proposed in reference [47] was used:

$$k_{T,PTFE} = 4.86 \times 10^{-4} T + 0.253 \quad (55)$$

Experimental data for platinum and carbon black were used to generate the polynomial equations computed by the model to calculate the thermal conductivity:

$$k_{T,Pt} = -5.275 \times 10^{-4} T^3 + 2.543 \times 10^{-5} T^2 - 2.321 \times 10^{-2} T + 77.85 \quad R^2 = 0.999 \quad (56)$$

$$k_{T,CB} = 1.048 \times 10^{-6} T^2 - 2.869 \times 10^{-3} T + 2.979 \quad R^2 = 0.998 \quad (57)$$

In the same way as electric conductivity the thermal conductivity of phosphoric acid also depends on temperature and concentration. From the data provided by Turnbull [48] it was possible to generate an equation which couples the concentration of phosphoric acid with the thermal conductivity. At any given concentration a linear expression was obtained between

k_{T,H_3PO_4} and T :

$$\lambda_{H_3PO_4} = \left(-2.606 \times 10^{-4} w_{H_3PO_4} + 1.190 \times 10^{-3} \right) T + \left(2.086 \times 10^{-1} w_{H_3PO_4}^2 - 3.718 \times 10^{-1} w_{H_3PO_4} + 3.213 \times 10^{-1} \right) \quad (58)$$

The thermal conductivities of the cell body (titanium grade 2), membrane and carbon paper (Toray carbon paper present in the GDL) were assumed to be temperature independent as a result of insufficient data:

Formatted: Line spacing: 1.5 lines

Formatted Table

Formatted: Indent: First line: 0.75 pt, Line spacing: 1.5 lines

Formatted: Line spacing: 1.5 lines

Formatted: Indent: First line: 0.75 pt

Formatted Table

Formatted: After: 1.7 pt

Formatted Table

Formatted Table

Formatted: Left

Formatted Table

- Membrane: $0.41 \text{ W K}^{-1} \text{ m}^{-1}$ [49, 50]
- Carbon paper: $1.7 \text{ W K}^{-1} \text{ m}^{-1}$ [44]
- Titanium grade 2: $16.4 \text{ W K}^{-1} \text{ m}^{-1}$ [43]

Formatted: Portuguese Portugal

To calculate the effective thermal conductivity of the porous media k_T (GDLs, MPLs, and catalyst layers) an equation proposed by Hashin and Shtrikman [51] in 1962 for isotropic medium was used:

$$k_T = -2k_{T,solid} + \frac{1}{\varepsilon / (2k_{T,solid} + k_{T,fluid}) + (1 - \varepsilon) / 3k_{T,solid}} \quad (59)$$

Formatted Table

Where, $k_{T,solid}$ is the effective thermal conductivity of the solid phase.

An average of the solid species thermal conductivity was obtained:

$$k_{T,solid} = \varepsilon_{PTFE} k_{T,PTFE} + \varepsilon_{CB} k_{T,CB} \quad \text{at the MPLs} \quad (60)$$

Formatted: Left

Formatted Table

$$k_{T,solid} = \varepsilon_{PTFE} k_{T,PTFE} + \varepsilon_{CB} k_{T,CB} + \varepsilon_{H_3PO_4} k_{T,H_3PO_4} + \varepsilon_{Pt} \lambda_{Pt} \quad \text{at the catalyst layers} \quad (61)$$

Where, ε_{PTFE} , ε_{CB} , $\varepsilon_{H_3PO_4}$ and ε_{Pt} are the volume fractions of PTFE, carbon black, phosphoric acid and platinum, respectively. In the GDL, $k_{T,solid}$ was equal to the conductivity of the carbon paper.

2.5 Solution Technique

To solve the governing equations COMSOL Multiphysics version 3.5 was used which is a finite element analyses and solver software. The computations were performed on a 64 bit Windows platform with 8 GB of RAM, and Intel Core 2 Quad 2.5 GHz processor. Geometry A was divided in 2240 mesh elements, 1536 were triangular and 1004 were quadrilateral. Geometry B was divided into 4913 mesh elements, 2073 were triangular and 2840 were quadrilateral. In the MEA and gas channels we used a quadrilateral refine mesh, in the other areas of the computational domain a triangular mesh with a growing rate of 1.8. The critical regions of the computational domain were the MEA and gas channels; to these regions was done refinement studies in previous works. With those studies we didn't find any significant numerical error. For example, when was used a much more refined mesh (with more 51% of degrees of freedom) the predicted current density only differed 0.2 mA cm^{-2} from the base case used in this work.

A direct parametric non-linear solver was applied, and the cell potential, V_{cell} , was used as the parametric variable.

3 Results and Discussion

3.1 Polarisation curve

Figure 5 compares model predictions with the corresponding experimental data for a PEM fuel cell utilising 50% Pt/C at the cathode and 20% Pt/C at the anode at 150 °C and at atmospheric pressure. The membrane PA doping level was 630 %. Air was used at the cathode and hydrogen at the anode. The open circuit potential (*OCP*) was obtained from Eq. (15), and was the same for both geometries, 1.16 V. Until 0.7 V a good agreement between experimental data and model results was obtained for both geometries. This region is characterized by low current densities and a sharp decrease in voltage due to activation losses, mainly in the cathode side. Below this potential the performance predicted for each geometry was different. The results predicted by the model agreed with the experimental data when geometry B was used. On the other hand, with geometry A the predicted performance was much lower than the experimental performance.

With Geometry B the polarization curve exhibited three different regions, identified in Figure 5. From open circuit to 0.7 V the potential rapidly decreased due to activation losses. Between 0.7 and 0.2 V the potential fell almost linearly with current density, as a result of Ohmic losses, caused by ionic and electronic resistance. In this particular system the electronic resistance was insignificant when compared with the ionic resistance in the catalyst layers and membrane. Typical values of ionic resistance for PBI doped with H₃PO₄ can be found in the work developed by Ma et al. [38]. They observed a value of 37.57 Ω cm for a doping level of 630%, at 150 °C, and 5% of relative humidity. Pure H₃PO₄ (species responsible for ionic conductivity in the catalyst layers) has typically an ionic resistance lower than that of PBI doped with H₃PO₄. At 150 °C and 99.72 %wt, MacDonald and Boyack [36], measured a value of 2.053 Ω cm. Both these values are higher than the electric resistance of carbon black, 0.222 Ω cm [41].

At potentials below 0.2 V there was a rapid fall in voltage. This was caused by mass transport limitations, in particular the oxygen diffusion and solubility in hot, concentrated phosphoric acid. The value of oxygen diffusion coefficient, given by Eq. (37), was very low for the entire range of potential, $1.08 \times 10^{-9} \text{ m}^2 \text{ s}^{-1}$. Similarly the solubility (Eq. (36)), was

Deleted: 4

Deleted: matched

Deleted: 4

Field Code Changed

Deleted: [37]

Field Code Changed

Deleted: [35]

Field Code Changed

Deleted: [46]

low, $3.75 \times 10^{-6} \text{ mol Pa}^{-1} \text{ m}^{-3}$, which contributed to the low limiting current density of 1.43 A cm^{-2} .

The performance predicted with Geometry A dropped sharply and linearly between potentials of 0.7 and 0 V, reaching a maximum of 0.46 A cm^{-2} . This unrealistic behaviour was caused by an inefficient utilization of the catalyst layers, due to the position of the boundary conditions (Eqs. (31)-(32)) to solve the conservation of charge for the solid phase (Eq. (9)). Figure 6 shows the current density profile at the cathode catalyst layer at 0.4 V for Geometry A. As shown the reaction did not occur uniformly through the catalyst layer. The maximum current density was obtained in the adjacent areas of the ribs, 0.725 A cm^{-2} , whilst, mid way between the ribs the current density was very low, 0.050 A cm^{-2} . The linear trend of the polarization curve below 0.7 V demonstrates that the electric and protonic resistance had a predominate effect. The electrons could only flow to the external circuit through small regions at the edges of the MEA, therefore, they experienced high electric resistance to flow from the reaction sites to the land thus the rate of the reactions decreased, mainly in the middle of the catalyst layers (farther region from the land).

Deleted: 5

Figure 7 shows the current density profile at 0.4 V at the cathode catalyst layer for Geometry B. In contrast with Geometry A the reaction rate was more uniform through the catalyst layer, due to the presence of the ribs between channels. The minimum current density was obtained at the edges of the catalyst layer, 0.085 A cm^{-2} . This low value was not caused by the electric resistance but by mass transport limitations, i.e. oxygen molecules could not reach these areas easily.

Deleted: 6

Figures 5 and 6 demonstrate that Geometry A is not suitable for fuel cell simulations. A realistic performance could only be achieved with the introduction of artificial boundary conditions at the interface GDL/Gas channel, which simulate the ribs effect. Such a simulation was done and the results are shown in Figure 8. With these new boundary conditions the area responsible for the electron diffusion from the MEA to the bipolar plates increases. For that reason, the current density was distributed more uniformly in the catalyst layer, leading to more realistic results.

Deleted: 4

Deleted: 5

Formatted: Line spacing: 1.5 lines

Deleted: obtained r

3.2 Non-isothermal operation

Electrochemical reactions within the fuel cell are exothermic; therefore, heat is released during operation, mainly in the cathode side. The resultant increased temperature causes two opposite effects. The *OCP* and thus cell performance decreases, caused by lower enthalpy

1 and higher entropy. On the other hand the exchange current density increases exponentially
2 and species transport in the gas phase also improves, i.e. performance increases. The
3 transport through hot and concentrate phosphoric acid is not easy to predict because it
4 depends on both temperature and water partial pressure. If the water partial pressure is
5 maintained constant or increases, then the diffusion in phosphoric acid also improves with
6 temperature.
7
8
9

10 To analyse to what extent the non-isothermal conditions affected performance, the results
11 predicted by the model were compared with results obtained at isothermal conditions. For
12 both cases the simulations were carried out for a PEM fuel cell utilising 50% Pt/C at the
13 cathode and 20% Pt/C at the anode at 150 °C and at atmospheric pressure. Air was used at
14 the cathode, hydrogen at the anode and Geometry B was used to perform the simulations.
15
16
17

18 Figure 9 shows the obtained cell voltage vs. current density behaviour. From open circuit
19 potential to 0.4 V the performance was very similar for both isothermal and non-isothermal
20 conditions. However below this point the non-isothermal model predicted a much better
21 performance. The limiting current for the non-isothermal case was 15% higher than the
22 isothermal case. This higher performance, at high currents indicates an improvement in
23 species transport, as can be seen in Table 3. The improvement in species transport can only
24 be explained by a significant temperature increase inside the fuel cell. Figure 10 shows the
25 average temperature of the MEA at different cell potentials. The temperature was practically
26 constant, at 150 °C until potentials of 0.6 V, however, below this potential the temperature
27 increased until a maximum of 181 °C at 0 V.
28
29
30
31
32
33

Deleted: 7

Deleted: 8

3.3 Local overpotential distribution

34
35
36
37 Figure 11 shows the local overpotential distribution predicted for a section of the cathode
38 catalyst layer at three different cell potentials (0.6 V, 0.4 V and 0.2 V). The simulations were
39 carried out for a PEM fuel cell utilising 50% Pt/C at the cathode and 20% Pt/C at the anode at
40 150 °C and at atmospheric pressure. Air was used at the cathode, hydrogen at the anode and
41 Geometry B was used to perform the simulations. From Figure 11 two general results can be
42 seen. The local overpotential was not uniform within the catalyst layer and the maximum was
43 always reached under the land. At 0.6 V the overpotential variation was nearly constant, the
44 difference between the maximum and minimum value was 2 mV. As the cell potential
45 decreased the overpotential variation increased, at 0.4 V the difference between the
46 maximum and minimum value was 14 mV, and at 0.2 V it reached 47 mV.
47
48
49
50
51
52
53
54
55
56
57
58
59
60

Deleted: 9

Deleted: 9

1 It can be concluded that the overpotential variation was small for the entire range of cell
 2 voltage; however, even small differences are important on performance prediction because it
 3 is related exponentially to the current density. This observation is important because it points
 4 out one big limitation of models that assume an uniform overpotential distribution. Examples
 5 of these models are those that assume the catalyst layer as a reactive boundary. This
 6 assumption can lead to an over predicted performance, especially at high current densities
 7 where the overpotential variation is higher.
 8
 9
 10
 11

12 3.4 Dead and active reaction zones

13
 14
 15 The distribution of the reactants reaction rate in the catalyst layers can be an efficient way
 16 to measure the effective active area of the catalyst layers. The reaction rate was calculated
 17 from the volumetric current density, as is demonstrated by Eq. (63),
 18
 19

$$20 \quad RR = \frac{j}{nF} \quad (62)$$

21
 22
 23
 24
 25 Where, RR is the reaction rate.

26
 27
 28 Figure 12 shows the oxygen reaction rate (ORR) distribution in the catalyst layer for
 29 Geometry B at two different positions (catalyst layer/MPL interface and catalyst
 30 layer/membrane interface) and at three different cell potentials (0.6 V, 0.4 V and 0.2 V). The
 31 simulations were carried out for a PEM fuel cell utilising 50% Pt/C at the cathode and 20%
 32 Pt/C at the anode at 150 °C and at atmospheric pressure. Air was used at the cathode and
 33 hydrogen at the anode. From Figure 12 the main feature can be seen was that ORR was non-
 34 uniform in both directions, it varied with thickness and length of the catalyst layer.
 35
 36
 37

38 It is evident that the variation in ORR distribution with the thickness of the catalyst layer,
 39 was more significant at high current densities. At 0.6 V the ORRs predicted by the model at
 40 the catalyst layer/MPL and catalyst layer/membrane interfaces were very similar, the mean
 41 values of both predictions only differed by 5.70 mol m⁻³ s⁻¹ (2.75 mA cm⁻² in terms of current
 42 density). On the other hand, at 0.2 V the predictions for these two interfaces were
 43 significantly different. The mean value predicted for the catalyst layer/MPL interface (3.49 x
 44 10³ mol m⁻³ s⁻¹) was 42% higher than the predicted value at the catalyst layer/membrane
 45 interface (2.03 x 10³ mol m⁻³ s⁻¹). These results suggest that the reaction at low potentials
 46 occurred mainly in the adjacent region to the MPL; near the membrane the catalyst layer can
 47 be considered a “dead zone”.
 48
 49
 50
 51
 52
 53
 54
 55
 56
 57
 58
 59
 60

Deleted: (63)

Deleted: (46)

Deleted: 62

Deleted: 46

Deleted: 10

Deleted: 10

As mentioned before the ORR also varies with the length of the catalyst layer. Two distinct regions can be observed in Figure 12. The first one corresponded to the extremities of catalyst layer. This region was characterized by very low values of ORR rate for all potential ranges. This means that oxygen molecules cannot diffuse easily to these regions, and as consequence the catalyst layer was not efficiently used. The second region is between the extremities of the catalyst layer. In this region the ORR distribution followed two distinct trends. At high potentials the ORR was nearly constant, however at low potentials the trend was a sinusoidal function with a maximum under the gas channel regions and a minimum under the land regions. Sun et al. [52] made a similar study for a Nafion system. At low potentials they found the same sinusoidal trend, with maximum ORR located under the flow channels. At these conditions the electrochemical reaction is very rapid; therefore, oxygen diffusion becomes the limiting factor. At high potentials Sun et al. observed that the maximum ORR moved from regions under the flow channel to regions under the land. This behaviour was caused by the low ORR; the oxygen molecules diffused fast enough to the reaction sites, therefore, the limiting factor was ohmic losses between the regions under the channel and under the land. This phenomenon was not observed in the present study; at high potentials the ORR was uniform. This fact can be explained by the higher solid phase conductivity used in this paper in comparison with the one used by Sun et al. Kulikovsky et al. [53] showed that the most active catalyst area was dependent on the choice of parameters, in particular the solid phase conductivity, k_s . They found that an increase of k_s leads to a more uniform distribution of the reaction rate. In this paper the average solid phase conductivity in the catalyst layer was 1000 times higher than the value used by Sun et al. due to the introduction of the platinum conductivity in the calculation of k_s .

3.5 Temperature distribution

The temperature distribution through the MEA is a very important consideration as it can give important information about the real temperature in the centre of the cell and it can be useful to predict possible problems concerning thermal stresses and hot spots.

In the apparatus used in our laboratory the temperature in the fuel cell was measured by a thermocouple embedded in the collector plates. The data collected by the thermocouple was used by an on/off control system to control the heaters. Figure 13 shows the temperature profile and the heat flux direction for Geometry B at 0.9 and 0 V. The simulations were

Deleted: 10

Field Code Changed

Deleted: [47]

Field Code Changed

Deleted: [48]

Deleted: 11

1 carried out for a PEM fuel cell utilising 50% Pt/C at the cathode and 20% Pt/C at the anode at
2 150 °C and at atmospheric pressure. Air was used at the cathode and hydrogen at the anode.
3
4

5
6 One main observation can be seen from Figure 13, is that the heat source shifted with
7 potential. At 0.9 V the heat source was located, as expected, at the heaters, however at 0 V
8 the heat source was located at the centre of the domain (MEA region). In addition, the
9 temperature distribution at 0.9 V was more uniform than at 0 V. The difference between the
10 two temperature limits at 0.9 V was 76 K, in contrast, at 0 V it was 116 K. The average
11 temperature of the MEA for the all range of potentials was shown in Figure 10. As can be
12 seen from Figure 8 the average temperature of the MEA at low potentials was much higher
13 than 150 °C. This meant that the temperature in the middle of the cells was not efficiently
14 controlled with the current location of the thermocouple. This feature can lead to phosphoric
15 acid dehydration and consequently a decrease in proton conductivity.
16
17

18
19 It is also important to analyse the temperature profile through the membrane in order to
20 detect possible hot spots or abnormal temperature differences. Figure 14 shows the
21 temperature profile predicted as a function of the membrane length at three different cell
22 potentials (0.6 V, 0.4 V and 0.2 V) for Geometry B. The trend in the temperature profile was
23 very similar to the ORR profile shown in Figure 12, which indicates the importance of the
24 reactive heat for the overall heat generation. Once more two distinct regions can be
25 identified. The first one was at the edges of the membrane. This region was characterised by
26 a sharp fall in temperature for the entire potential range. At 0.2 V the temperature fell from
27 449 K to 432 K, a large difference for such a small distance (8×10^{-3} m). This temperature
28 difference could lead to degradation problems due to thermal stress. Between the edges of the
29 membrane, the temperature was constant at high potentials but at low potentials it was non-
30 uniform and followed a sinusoidal trend with hot spots under the channel regions. The
31 temperature difference between the regions under the flow channel and the land was not so
32 marked at that at the membrane edges (only 3 K at 0.2 V), therefore thermal degradation
33 problems in middle regions of the membrane are less likely to occur.
34
35

36
37 To further illustrate the impact of the reactive heat on the overall heat generation and
38 consequently the temperature profile, the total reactive and ohmic heat were calculated and
39 represented as a function of the cell potential in Figure 15. Both reactive and ohmic heat
40 increased as the potential decreased as a result of a greater current density. However, the
41 Ohmic heat at low potentials was low when compared with reactive heat; for example at 0.2
42 V it only corresponded to 12.2% of the total heat. This explains why the temperature profile
43
44
45
46
47
48
49
50
51
52

Deleted: 11

Deleted: 8

Deleted: 12

Deleted: 10

Deleted: 13

1 through the membrane length was similar to the ORR profile through the catalyst layer
2 length.
3
4
5

6 4 Conclusions 7 8

9 A two dimensional agglomerate model was developed to simulate the performance of an
10 intermediate temperature PEMFC equipped with a phosphoric acid doped PBI membrane.
11 The model was capable of predicting the polarization performance, temperature distribution
12 and all transport characteristics.
13
14

15 Two different geometries were analysed and the results compared. It was found that the
16 model predictions are highly dependent on the adopted geometry. It became clear that
17 Geometry A (along the channel direction) was only suitable for fuel cell modelling with the
18 introduction of artificial boundary conditions at the GDL/gas channel interface that simulates
19 the land effect. On the other hand, Geometry B (cross the channel direction) was able to
20 simulate the general trend in fuel cell performance and, in addition, the simulation
21 predictions matched the experimental results. The effect of the non-isothermal conditions on
22 performance was investigated and compared with the results obtained at isothermal
23 conditions. It was concluded that the performance increased when non-isothermal conditions
24 were used in the simulations. This fact was caused by a substantial temperature increase of
25 the MEA at high current densities, leading to an improvement of transport properties.
26
27
28
29
30

31 It was also found that the local overpotential distribution and the oxygen reaction rate
32 were non-uniform through the catalyst layer. The maximum reaction rate was obtained under
33 the channel regions and the lower rate was obtained at the edges of the MEA. This feature,
34 leads to large temperature difference between the central regions and the edges of the MEA.
35 The temperature difference becomes potentially very problematic at the membrane because it
36 could lead to thermal degradation due to thermal stresses. From the analyses of the oxygen
37 reaction rate it was shown that the catalyst layer was not efficiently used. In particular, the
38 extreme regions of the catalyst layer had a very low reaction rate for the all ranges of
39 potential, this region represents 15% of the total catalyst layer volume.
40
41
42
43
44
45

46 Acknowledgements 47

48 The authors acknowledge the support of EPSRC through the Supergen; fuel cell
49 consortium award.
50

51 Deleted: ¶
52
53
54
55
56
57
58
59
60

Appendix A

In the electrochemical reactions there are three different participants: electrons, protons and gas reactant/products. The reaction only takes place on the catalyst surface where all the three species have access. The electrons travel through the electric conductive solids, the protons through the electrolyte (phosphoric acid in this particular system) and the gas species should have an easy access to the reaction sites. In order to enhance performance and to reduce platinum loading the catalyst structure should maximise the three phase boundary formed by the electrolyte, solid and void phases. To simulate all the transport and electrochemical processes within the catalyst layer the model treats it as spherical agglomerates of catalyst particles with porous inter-agglomerate space, where each agglomerate is covered by a thin film of electrolyte.

The geometric parameters of the catalyst layer and agglomerate are strongly dependent on the fabrication process. Therefore is not easy to find consensual values in the literature. The thickness of the catalyst layers was measured from the analyses of scanning electron micrograph (SEM) images. For cathodes with $0.4 \text{ mg}_{\text{Pt}} \text{ cm}^{-2}$, of 50% Pt/C, and 40% wt_{PTFE} the average thickness was $12.5 \text{ }\mu\text{m}$ and for anodes with $0.2 \text{ mg}_{\text{Pt}} \text{ cm}^{-2}$, 20% Pt/C, and 40% wt_{PTFE} the average thickness was $13.8 \text{ }\mu\text{m}$. In this paper an average value of $0.5 \text{ }\mu\text{m}$ was adopted for the agglomerate diameter. A wide range of values have been reported in literature, Broka and Ekdunge [28] estimated the agglomerate diameter to be between 1 and 5 μm through the analyses of SEM images. Using the same technique Siegel et al. [54] reported an average value of $6.1 \text{ }\mu\text{m}$. On another hand Ihonen et al. [55] estimated a much lower value using scanning transmission electron microscopy images, $0.11 \text{ }\mu\text{m}$. Following the same trend different values for the electrolyte fraction in the agglomerate have been proposed. For example, Sun et al. [52] used a value of 0.5 and Jaouen et al. [56] used 0.3. In this paper we used an average value of 0.3. To calculate the thickness of the electrolyte film the next equation was proposed:

$$\delta = \left\{ \left[\frac{\left(\frac{L_{\text{H}_3\text{PO}_4}}{\rho_{\text{H}_3\text{PO}_4}} A - \frac{\varepsilon_{\text{agg}} V_{\text{solids}}}{1 - \varepsilon_{\text{agg}}} \right) (1 - \varepsilon_{\text{agg}}) V_{\text{agg}}}{V_{\text{solids}}} + V_{\text{agg}} \right] \frac{3}{4\pi} \right\}^{\frac{1}{3}} - r_{\text{agg}} \quad (63)$$

Field Code Changed

Field Code Changed

Deleted: [49]

Field Code Changed

Deleted: [50]

Field Code Changed

Deleted: [47]

Field Code Changed

Deleted: [51]

Deleted: 63

Deleted: 47

Where, $L_{H_3PO_4}$ is the mass of phosphoric acid per area, A is the catalyst layer area (9 cm²), V_{solids} is the total volume of solids (platinum, carbon black, and PTFE) in the catalyst layer, and V_{agg} is the agglomerate volume. The effective porosity of the catalyst layers will depend on the amount of phosphoric acid inside the catalyst layers.

Knowing the geometric properties of the catalyst layer and agglomerate the following procedure was adopted to describe the transport and electrochemical reaction processes. [ref, ref]

In the catalyst layers the reactants are transported to the catalyst surface as molecular species dissolved in phosphoric acid. The concentration at the gas-liquid interface was obtained by Henry's Law.

$$C_{i\,gll} = H_i p_i \quad (64)$$

Deleted: 64

Deleted: 48

Where, H_i is the Henry constant, and p_i is the partial pressure of the reactants.

The reactant mass balance in the catalyst layer was described by the following equivalent equations:

$$\nabla N_i + a_{agg} N_i' = 0 \quad (65)$$

Deleted: 65

Deleted: 49

$$\nabla N_i + R_i = 0 \quad (66)$$

Deleted: 66

Deleted: 50

Where, N_i is the overall reactants mole flux, N_i' is the reactants mole flux in the phosphoric acid film, and R_i is the reaction rate.

The transport in the liquid phase could be described by Fick's Law:

$$N_i' = D_{liq,i} \frac{\partial C_i}{\partial r} \quad (67)$$

Deleted: 67

Deleted: 51

Where, C_i is the reactants concentration, and r is the radius.

It was assumed that the phosphoric acid film was present in the agglomerate evenly, and the thickness of the film was much smaller than the size of the agglomerate. Therefore the reactant flux can be described by the following equation:

$$N_i' = D_{liq,i} \frac{(C_{i\,gll} - C_{i\,lls})}{\delta} \quad (68)$$

Deleted: 68

Deleted: 52

Where, $C_{i\,lls}$ is the reactants concentration at the surface of the agglomerate.

The overall oxygen reduction reaction and hydrogen oxidation reaction was assumed to follow first-order kinetics with respect to the reactant concentration [52, 57]:

$$R_i = k_c C_i \quad (69)$$

Field Code Changed

Deleted: [47, 52]

Deleted: 69

Deleted: 53

The previous equation can be simplified if the overall reaction rate only depends on the reactant concentration at the outer surface of agglomerate.

$$R_{agg,i} = E_r k_c C_{i,l/s} (1 - \varepsilon_{CAT}) \quad (70)$$

Deleted: 70

Deleted: 54

Where, $R_{agg,i}$ is the reaction rate based on the agglomerate volume, and E_r is the effectiveness factor. However to apply this approximation it is necessary to introduce a new factor which takes into account the geometry of the agglomerate and the diffusion resistance of reactant molecules inside the agglomerate. This factor is the effectiveness, which can be described, for spherical agglomerate, by the following equation [58]:

$$E_r = \frac{3}{\Phi} \left(\frac{1}{\tanh(\Phi)} - \frac{1}{\Phi} \right) \quad (71)$$

Deleted: [53]

Field Code Changed

Deleted: 71

Deleted: 55

Where, Φ is an adimensional number called the Thiele's modulus:

$$\Phi = r_{agg} \sqrt{\frac{k_c}{D_{liq,i}^{eff}}} \quad (72)$$

Deleted: 72

Deleted: 56

Where, $D_{liq,i}^{eff}$ is the effective reactants diffusion inside the agglomerate.

The oxygen consumption rate was related to the current density according to:

$$j = nFR_i = nFR_{agg,i} (1 - \varepsilon_{CAT}) = nFE_r k_c (1 - \varepsilon_{CAT}) C_{i,l/s} \quad (73)$$

Deleted: 73

Deleted: 57

Deleted: (68)

Deleted: (52)

From Eq. (68):

$$C_{i,l/s} = - \frac{N_i (r_{agg} + \delta) \delta + D_{liq,i} r_{agg} C_{i,g/l}}{D_{liq,i} r_{agg}} \quad (74)$$

Deleted: 74

Deleted: 58

Deleted: (66)

Deleted: (50)

From Eqs.s (66)-(70):

$$N_i = \frac{E_r k_c C_{i,l/s} (1 - \varepsilon_{CAT})}{a_{agg}} \quad (75)$$

Deleted: (70)

Deleted: (54)

Deleted: (75)

Deleted: 59

From Eqs. (74)-(75):

$$C_{i,l/s} = C_{i,g/l} \left[1 + \frac{E_r k_c (1 - \varepsilon_{CAT}) (r_{agg} + \delta) \delta}{r_{agg} a_{agg} D_{liq,i}} \right]^{-1} \quad (76)$$

Deleted: (74)

Deleted: (58)

Deleted: (75)

Deleted: (59)

Deleted: 76

Deleted: 60

The volumetric current density, j , described by Eq. (12) was obtained through the combination of Eqs. (73)-(76). The reaction rate (Eq. (13)) was obtained from Eqs. (11)-(73).

Deleted: (73)

Deleted: (57)

Deleted: (76)

Deleted: (60)

Deleted: (73)

Deleted: (57)

Deleted: ¶

Formatted: Line spacing: 1.5 lines

List of Symbols

1	
2	
3	
4	a_{agg} Effective agglomerate surface area (m^{-1})
5	a_{pt} Electrocatalytic surface area (m^{-1})
6	C Concentration ($mol\ m^{-3}$)
7	c_p Mixture average specific heat capacity ($J\ kg^{-1}\ K^{-1}$)
8	D Binary diffusivity for gas phase multicomponent mixture ($m^2\ s^{-1}$)
9	D_{liq} Reactants diffusivity in hot phosphoric acid ($m^2\ s^{-1}$)
10	E_r Effectiveness factor
11	F Faraday's constant ($C\ mol^{-1}$)
12	i_o Exchange current density ($A\ m^{-2}$)
13	j Volumetric current density ($A\ m^{-3}$)
14	H Henry constant ($mol\ m^{-3}\ Pa^{-1}$)
15	\bar{h} Local convective heat transfer coefficient ($W\ m^{-2}\ K^{-1}$)
16	k_c Reaction rate constant (s^{-1})
17	k_{elect} Protonic Conductivity ($S\ m^{-1}$)
18	k_e Electric Conductivity ($S\ m^{-1}$)
19	k_T Thermal conductivity ($W\ m^{-1}\ K^{-1}$)
20	K Permeability of gas diffusion layers or catalyst layers (m^2)
21	M <u>Molecular weight ($kg\ mol^{-1}$)</u>
22	n Number of transfer electrons
23	N Mole flux ($mol\ m^{-2}\ s^{-1}$)
24	N' Mole flux in the phosphoric acid film ($mol\ m^{-2}\ s^{-1}$)
25	\overline{Nu} Nusselt number
26	p Pressure (Pa)
27	q_{conv} Convective heat flux ($W\ m^{-2}$)
28	q_{Joule} Joule heating ($W\ m^{-3}$)
29	Pr Prandtl number
30	$q_{reaction}$ Heat of reaction ($W\ m^{-3}$)
31	p_{sat} Saturation pressure of water (Pa)
32	R Universal gas constant ($J\ mol^{-1}\ K^{-1}$)
33	R_{agg} Reaction rate based on agglomerate volume ($mol\ m^{-3}\ s^{-1}$)
34	r_{agg} Agglomerate radius (m)
35	R_{CAT} Reaction rate based on catalyst layer volume ($mol\ m^{-3}\ s^{-1}$)
36	Re_{local} Local Reynolds number
37	S Electrocatalytic specific surface area (m^{-1})
38	St Source term
39	T Temperature (K)
40	T_{air} Temperature of the exterior air (K)
41	V Catalyst layer volume (m^3)
42	v Velocity vector ($m\ s^{-1}$)
43	V_{ref} Reference potential (V)
44	w Mass fraction
45	x Mole fraction
46	Greek letters
47	α Transfer coefficient
48	δ Thin film thickness (m)
49	ΔS Entropy ($J\ mol^{-1}\ K^{-1}$)
50	ε Porosity
51	η Overpotential (V)
52	μ Viscosity (Pa s)
53	ρ Density ($kg\ m^{-3}$)
54	Γ Deviatoric strain rate
55	ϕ Potential (V)
56	Φ Thiele's modulus
57	Superscripts and Subscripts
58	a Anode
59	agg Agglomerate
60	c Cathode
	CAT Catalyst layer

Formatted: Superscript

<i>e</i>	Conservation of energy
<i>eff</i>	Effective
<i>elect</i>	Electrolyte
<i>i</i>	Reactants, H ₂ or O ₂
<i>ref</i>	Reference conditions
<i>s</i>	Solid
ϕ	Conservation of charge

References

- [1] J. S. Wainright, et al., *J. Electrochem. Soc.*, **1995**, *142*, L121.
- [2] J.-T. Wang, et al., *Electrochim. Acta*, **1996**, *41*, 193.
- [3] S. R. Samms, et al., *J. Electrochem. Soc.*, **1996**, *143*, 1225.
- [4] Y.-L. Ma, et al., *J. Electrochem. Soc.*, **2004**, *151*, A8.
- [5] Z. Qi and S. Buelte, *J. Power Sources*, **2006**, *161*, 1126.
- [6] P. Jannasch, *Curr. Opin. Colloid Interface Sci.*, **2003**, *8*, 96.
- [7] I. Honma, et al., *J. Electrochem. Soc.*, **2003**, *150*, A616.
- [8] S.-H. Kwak, et al., *Solid State Ionics*, **2003**, *160*, 309.
- [9] H. Kim, et al., *Macromol. Rapid Commun.*, **2004**, *25*, 1410.
- [10] V. Ramani, et al., *J. Membr. Sci.*, **2004**, *232*, 31.
- [11] S.-H. Kwak, et al., *Electrochim. Acta*, **2004**, *50*, 653.
- [12] E. K. Pefkianakis, et al., *Macromol. Rapid Commun.*, **2005**, *26*, 1724.
- [13] J. A. Asensio and P. Gomez-Romero, *Fuel Cells*, **2005**, *5*, 336.
- [14] L. Xiao, et al., *Fuel Cells*, **2005**, *5*, 287.
- [15] V. Baglio, et al., *J. Electrochem. Soc.*, **2005**, *152*, A1373.
- [16] L. Paturzo, et al., *Catal. Today*, **2005**, *104*, 213.
- [17] M. Li, et al., *Electrochem. Solid-State Lett.*, **2006**, *9*, A60.
- [18] D. M. Bernardi and M. W. Verbrugge, *AIChE J.*, **1991**, *37*, 1151.
- [19] L. Ma, et al., *Journal of Fuel Cell Science and Technology*, **2005**, *2*, 246.
- [20] D. Cheddie and N. Munroe, *Journal of Power Sources*, **2005**, *147*, 72.
- [21] A. Biyikoglu, *Int. J. Hydrogen Energy*, **2005**, *30*, 1181.
- [22] A. R. Korsgaard, et al., *J. Power Sources*, **2006**, *162*, 239.
- [23] D. Cheddie and N. Munroe, *Energy Convers. Manage.*, **2006**, *47*, 1490.
- [24] D. Cheddie and N. Munroe, *J. Power Sources*, **2006**, *156*, 414.
- [25] D. Cheddie and N. Munroe, *J. Power Sources*, **2006**, *160*, 215.
- [26] D. Cheddie and N. Munroe, *Int. J. Hydrogen Energy*, **2007**, *32*, 832.
- [27] K. Scott, et al., *J. Appl. Electrochem.*, **2007**, *37*, 1245.
- [28] K. Broka and P. Ekdunge, *J. Appl. Electrochem.*, **1997**, *27*, 281.
- [29] M. Mamlouk and K. Scott, *Int. J. Hydrogen Energy*, **35**, 784.
- [30] J. A. Ochoa-Tapia and S. Whitaker, *Int. J. Heat Mass Transfer*, **1995**, *38*, 2647.
- [31] H. C. Brinkman, *Appl. Sci. Res.*, **1949**, *1*, 27.
- [32] M. J. Lampinen and M. Fomino, *J. Electrochem. Soc.*, **1993**, *140*, 3537.
- [33] F. P. Incropera and F. P. Incropera, *Fundamentals of heat and mass transfer*, John Wiley, Hoboken, NJ, **2007**.
- [34] T. Sousa, et al., *Chem. Eng. Sci.*, **65**, 2513.
- [35] K. Klinedinst, et al., *J. Electroanal. Chem.*, **1974**, *57*, 281.
- [36] D. I. MacDonald and J. R. Boyack, *J. Chem. Eng. Data*, **1969**, *14*, 380.
- [37] R. Bouchet and E. Siebert, *Solid State Ionics*, **1999**, *118*, 287.
- [38] Y. L. Ma, et al., *J. Electrochem. Soc.*, **2004**, *151*.
- [39] Carbon Paper, can be found under http://www.torayca.com/properties/en/images/report_eng09_2.html, **2005**.
- [40] T. Zhou and H. Liu, *J. Power Sources*, **2006**, *161*, 444.

Formatted	...	[1]
Formatted: Indent: Before: 0 pt, First line: 0 pt		
Formatted	...	[2]
Formatted	...	[3]
Formatted	...	[4]
Formatted	...	[5]
Formatted	...	[6]
Formatted	...	[7]
Formatted	...	[8]
Formatted	...	[9]
Formatted	...	[10]
Formatted	...	[11]
Formatted	...	[12]
Formatted	...	[13]
Formatted	...	[14]
Formatted	...	[15]
Formatted	...	[16]
Formatted	...	[17]
Formatted	...	[18]
Formatted	...	[19]
Formatted	...	[20]
Formatted	...	[21]
Formatted	...	[22]
Formatted	...	[23]
Formatted	...	[24]
Formatted	...	[25]
Formatted	...	[26]
Formatted	...	[27]
Formatted	...	[28]
Formatted	...	[29]
Formatted	...	[30]
Formatted	...	[31]
Formatted	...	[32]
Formatted	...	[33]
Formatted	...	[34]
Formatted	...	[35]
Formatted	...	[36]
Formatted	...	[37]
Formatted	...	[38]
Formatted	...	[39]
Formatted	...	[40]

[41] D. Pantea, et al., *Appl. Surf. Sci.*, **2003**, *217*, 181.
 [42] R. W. Powell and R. P. Tye, *British Journal of Applied Physics*, **163**, *14*, 662.
 [43] ASM Material Data Sheet, can be found under <http://asm.matweb.com/search/SpecificMaterial.asp?bassnum=MTU020>, **2009**.
 [44] Carbon Paper, can be found under www.torayca.com, **2005**.
 [45] C. R. Wilke, *The Journal of Chemical Physics*, **1950**, *18*, 517.
 [46] R. H. Perry, et al., *Perry's chemical engineers' handbook*, McGraw-Hill, New York, **1997**.
 [47] J. Brandrup, et al., *Polymer handbook*, Wiley, New York, **1999**.
 [48] A. G. Turnbull, *J. Chem. Eng. Data*, **1965**, *10*, 118.
 [49] Polybenzimidazole (PBI) Material Information can be found under <http://www.goodfellow.com/E/Polybenzimidazole.HTML>.
 [50] Data Sheets, can be found under http://www.plasticsintl.com/datasheets/797942226Celazole_PBI.pdf.
 [51] Z. Hashin and S. Shtrikman, *Journal of the Mechanics and Physics of Solids*, **1962**, *10*, 343.
 [52] W. Sun, et al., *Electrochim. Acta*, **2005**, *50*, 3359.
 [53] A. A. Kulikovskiy, et al., *J. Electrochem. Soc.*, **1999**, *146*, 3981.
 [54] N. P. Siegel, et al., *J. Power Sources*, **2003**, *115*, 81.
 [55] J. Ihonen, et al., *J. Electrochem. Soc.*, **2002**, *149*.
 [56] F. Jaouen, et al., *J. Electrochem. Soc.*, **2002**, *149*.
 [57] K. Karan, *Electrochem. Commun.*, **2007**, *9*, 747.
 [58] J. M. Thomas and W. J. Thomas, *Introduction to the principles of heterogeneous catalysis*, Academic Press, London ; New York, **1967**.
 [59] G. Welsch, et al., *Materials properties handbook: titanium alloys* ASM International **1994**.
 [60] W. Vogel, et al., *Electrochim. Acta*, **1974**, *20*, 79.
 [61] J. MacBreen, et al., *J. Electrochem. Soc.*, **1984**, *131*, 1215.
 [62] B. R. Scharifker, et al., *J. Electrochem. Soc.*, **1987**, *134*, 2714.
 [63] Z. Liu, et al., *Electrochim. Acta*, **2006**, *51*, 3914.
 [64] E. Birgersson, et al., *J. Electrochem. Soc.*, **2005**, *152*.

Formatted ... [41]
 Formatted ... [42]
 Formatted ... [43]
 Formatted ... [44]
 Formatted ... [45]
 Formatted ... [46]
 Formatted ... [47]
 Formatted ... [48]
 Formatted ... [49]
 Formatted ... [50]
 Formatted ... [51]
 Formatted ... [52]
 Formatted ... [53]
 Formatted ... [54]
 Formatted ... [55]
 Formatted ... [56]
 Formatted ... [57]
 Formatted ... [58]
 Formatted ... [59]
 Formatted ... [60]
 Formatted ... [61]
 Formatted ... [62]
 Formatted ... [63]
 Formatted ... [64]
 Formatted: Indent: Before: 0 pt, Hanging: 36 pt
 Deleted: [1] . J. S. Wainright, J.-T. Wang, D. Weng, R. F. Savinell and M. Litt, *J. Electrochem. Soc.* 1995, *142*, L121.¶
 [2] . J.-T. Wang, R. F. Savinell, J. Wainright, M. Litt and H. Yu, *Electrochim. Acta* 1996, *41*, 193.¶
 [3] . S. R. Samms, S. Wasmus and R. F. Savinell, *J. Electrochem. Soc.* 1996, *143*, 1225.¶
 [4] . Y.-L. Ma, J. S. Wainright, M. H. Litt and R. F. Savinell, *J. Electrochem. Soc.* 2004, *151*, A8.¶
 [5] . Z. Qi and S. Buelte, *J. Power Sources* 2006, *161*, 1126.¶
 [6] . P. Jannasch, *Curr. Opin. Colloid Interface Sci.* 2003, *8*, 96.¶
 [7] . I. Honma, H. Nakajima, O. Nishikawa, T. Sugimoto and S. Nomura, *J. Electrochem. Soc.* 2003, *150*, A616.¶
 [8] . S.-H. Kwak, T.-H. Yang, C.-S. Kim and K. H. Yoon, *Solid State Ionics* 2003, *160*, 309.¶
 [9] . H. Kim, S. An, J. Kim, J. Moon, S. Cho, Y. Eun, H.-K. Yoon, Y. Park, H.-J. Kweon and E.-M. Shin, *Macromol. Rapid Commun.* 2004, *25*, 1410.¶
 [10] . V. Ramani, H. R. Kunz and J. M. Fenton, *J. Membr. Sci.* 2004, *232*, 31.¶
 [11] . S.-H. Kwak, T.-H. Yang, C. ... [65]

Deleted: 1
 Deleted: 1
 Deleted: [29]

Tables

Table 1. Operational and geometric parameters for base case

Operational temperature	423.15	K
Operational pressure	101325	Pa
Channel length	2.90×10^{-2}	m
Channel width	1.5×10^{-3}	m
Channel deep	1.5×10^{-3}	m
Rib thickness	1×10^{-3}	m
GDL thickness	1.75×10^{-4} [39]	m
MPL thickness	2.15×10^{-5}	m
Membrane thickness	4.00×10^{-5}	m
Cathode catalyst layer thickness	1.25×10^{-5}	m
Anode catalyst layer thickness	1.38×10^{-5}	m

Table 2 Physical and electrochemical parameters for base case

Titanium			
Electric conductivity	7.407 x 10 ⁵ [59]		S m ⁻¹
Thermal conductivity	7.5 [59]		W m ⁻¹ K ⁻¹
PTFE			
Thermal conductivity	2.5 x 10 ⁻¹ [47]		W m ⁻¹ K ⁻¹
Membrane			
Protonic conductivity	Eq. (42)		S m ⁻¹
Thermal conductivity	40 [26]		W m ⁻¹ K ⁻¹
GDL			
Porosity	0.78 [39]		
Permeability	3.01 x 10 ^{-11a)}		m ²
Electric conductivity	1250 [39]		S m ⁻¹
Thermal conductivity	$-2k_{T,solid}+(\epsilon)/(2k_{T,solid}+k_{T,fluid})+(1-\epsilon)/3k_{T,solid}$ [40]		W m ⁻¹ K ⁻¹
MPL			
Porosity	0.6		
Permeability	1.97 x 10 ^{-12a)}		m ²
Electric conductivity	$k_s(2-\epsilon)/(\epsilon+2) \cdot k_z(2-2\epsilon)/(\epsilon+2)$ [40]		S m ⁻¹
Thermal conductivity	$-2k_{T,solid}+(\epsilon)/(2k_{T,solid}+k_{T,fluid})+(1-\epsilon)/3k_{T,solid}$ [40]		W m ⁻¹ K ⁻¹
Catalyst layers			
	Anode	Cathode	
Pt loading	2 x 10 ⁻³	4 x 10 ⁻³	Kg m ⁻²
Exchange current density	1.44 x 10 ³ [60]	2.63 x 10 ⁻⁴ [61]	A m _{Pt} ⁻²
Gama	1 [60]	1 [62, 63]	
Transfer coefficient	0.5 [60]	0.74	
Activation energy	16.9 x 10 ³ [60]	72.4 x 10 ³ [64]	J mol ⁻¹
Permeability	2.96 x 10 ^{-13a)}		m ²
Electric conductivity	$k_s(2-\epsilon)/(\epsilon+2)$ [40]		S m ⁻¹
Protonic conductivity	Eq. (45)		S m ⁻¹
Thermal conductivity	$-2k_{T,solid}+(\epsilon)/(2k_{T,solid}+k_{T,fluid})+(1-\epsilon)/3k_{T,solid}$ [40]		W m ⁻¹ K ⁻¹

^aCalculated from experimental data

^b k_s and $k_{T,solid}$ were treated as dependent variables.

Table 3 Transport properties at isothermal and non-isothermal conditions

	Non-isothermal	Isothermal	
Binary diffusion for O ₂ and H ₂ O	5.07 x 10 ^{-5b)}	4.85 x 10 ⁻⁵	m ² s ⁻¹
Binary diffusion for O ₂ and N ₂	3.97 x 10 ^{-5b)}	3.80 x 10 ⁻⁵	m ² s ⁻¹
Binary diffusion for N ₂ and H ₂ O	4.98 x 10 ^{-5b)}	4.71 x 10 ⁻⁵	m ² s ⁻¹
Solubility of O ₂ in H ₃ PO ₄	3.75 x 10 ^{-6b)}	3.64 x 10 ^{-6*}	mol Pa ⁻¹ m ⁻¹
Diffusion of O ₂ in H ₃ PO ₄	1.08 x 10 ^{-9b)}	8.55 x 10 ^{-10*}	m ² s ⁻¹

^bAverage value of the entire potential range

Deleted: 2
Deleted: 2
Deleted: [38]
Field Code Changed
Field Code Changed
Deleted: [38]
Deleted: [39]
Field Code Changed
Formatted: ... [66]
Deleted: (42)
Formatted: ... [67]
Deleted: (42)
Field Code Changed
Deleted: [29]
Deleted: [29]
Field Code Changed
Deleted: [40]
Field Code Changed
Deleted: [40]
Field Code Changed
Deleted: [40]
Field Code Changed
Deleted: [40]
Field Code Changed
Deleted: [41]
Field Code Changed
Deleted: [42]
Field Code Changed
Deleted: [41]
Field Code Changed
Deleted: [43, 44]
Field Code Changed
Deleted: [41]
Field Code Changed
Deleted: [41]
Field Code Changed
Formatted: Superscript
Deleted: [45]
Field Code Changed
Deleted: [40]
Formatted: ... [68]
Deleted: (45)
Formatted: ... [69]
Deleted: (45)
Field Code Changed
Deleted: [40]
Formatted: ... [70]
Deleted: 3
Deleted: 3

Figures Caption

- Fig. 1. Schematic representation of [computational domain, Geometry A](#).
- Fig. 2. Schematic representation of the computational domain, [Geometry A](#).
- Fig. 3. Schematic representation of the computational domains, [Geometry B](#).
- Fig. 4. Reactants and products mass fraction at gas channel/collector plate interface predicted at isothermal conditions for a PEMFC utilising 50% Pt/C at the cathode and 20% Pt/C at the anode at 150 °C and at atmospheric pressure. Air was used at the cathode and hydrogen at the anode. (A) — H₂ mass fraction, (B) — O₂ mass fraction, (C) — H₂O mass fraction.
- Fig. 5. Comparison between modelled and experimental data for a PEMFC utilising 50% Pt/C at the cathode and 20% Pt/C at the anode. Air was used at the cathode and hydrogen at the anode at atmospheric pressure. The controller set point was 150 °C. (A) — experimental data, (B) ♦ model results using Geometry B, (C) ▲ model results using Geometry A.
- Fig. 6. Current density profile at the cathode catalyst layer for Geometry A at 0.4 V. The simulation was carried out for PEMFC utilising 50% Pt/C at the cathode and 20% Pt/C at the anode. Air was used at the cathode and hydrogen at the anode at atmospheric pressure. The controller set point was 150 °C.
- Fig. 7. Current density profile at the cathode catalyst layer for Geometry B at 0.4 V. The simulation was carried out for PEMFC utilising 50% Pt/C at the cathode and 20% Pt/C at the anode. Air was used at the cathode and hydrogen at the anode at atmospheric pressure. The controller set point was 150 °C.
- Fig. 8. Comparison between modelled and experimental data for a PEMFC utilising 50% Pt/C at the cathode and 20% Pt/C at the anode. Air was used at the cathode and hydrogen at the anode at atmospheric pressure. The controller set point was 150 °C. (A) — experimental data, (B) ■ model results using Geometry A with the ribs effect.
- Fig. 9. Comparison between modelled and experimental data for a PEMFC utilising 50% Pt/C at the cathode and 20% Pt/C at the anode. Air was used at the cathode and hydrogen at the anode at atmospheric pressure. The controller set point was 150 °C. (A) — experimental data, (B) ♦ model results using Geometry B at non-isothermal conditions, (C) ▲ model results using Geometry B at isothermal conditions.
- Fig. 10. Predicted average temperature of the MEA for a PEMFC utilising 50% Pt/C at the cathode and 20% Pt/C at the anode. Air was used at the cathode and hydrogen at the anode at atmospheric pressure. The controller set point was 150 °C.
- Fig. 11. Local overpotential distribution in a section of the catalyst layer under three different cell potential for a PEMFC utilising 50% Pt/C at the cathode and 20% Pt/C at the anode. Air was used at the cathode and hydrogen at the anode at atmospheric pressure. The controller set point was 150 °C. A) 0.6 V, B) 0.4 V, C) 0.2 V.
- Fig. 12. O₂ reaction rate distribution of the catalyst layer under three different cell potential and at two different positions of the catalyst layer for a PEMFC utilising 50% Pt/C at the cathode and 20% Pt/C at the anode. Air was used at the cathode and hydrogen at the anode at atmospheric pressure. The controller set point was 150 °C. A) 0.6 V, B) 0.4 V, C) 0.2 V. (A) — catalyst layer/MPL interface, — catalyst layer/Membrane interface.
- Fig. 13. Temperature distribution and heat flux direction under two different cell potential for a PEMFC utilising 50% Pt/C at the cathode and 20% Pt/C at the anode. Air was used at the cathode and hydrogen at the anode at atmospheric pressure. The controller set point was 150 °C. A) 0.9 V, B) 0 V.

Deleted: 1

Deleted: 1

Deleted: the PEMFC. A – Geometry A, B – Geometry B

Deleted: a detail of

Deleted: 3

Deleted: 2

Deleted: . A) Geometry A, B) Geometry B.

Deleted: 4

Deleted: 3

Deleted: 5

Deleted: 4

Deleted: 6

Deleted: 5

Deleted: 7

Deleted: 6

Formatted: Font color: Auto

Deleted: ¶

Deleted: 9

Deleted: 7

Deleted: ¶

Formatted: Font: 12 pt, Not Bold, Complex Script Font: 12 pt

Deleted: 10

Deleted: 8

Deleted: 11

Deleted: 9

Deleted: 12

Deleted: 10

Deleted: 13

Deleted: 11

1 | Fig. 14 Temperature distribution of the membrane under three different cell potential for a
2 | PEMFC utilising 50% Pt/C at the cathode and 20% Pt/C at the anode. Air was used at the
3 | cathode and hydrogen at the anode at atmospheric pressure. The controller set point was 150
4 | °C. (A) — 0.2 V, (B) — 0.4 V, (C) — 0.6 V.

Deleted: 14

Deleted: 12

5 | Fig. 15 Total heat released during the operation of a PEMFC utilising 50% Pt/C at the
6 | cathode and 20% Pt/C at the anode. Air was used at the cathode and hydrogen at the anode at
7 | atmospheric pressure. The controller set point was 150 °C. (A) — total heat, (B) —
8 | reactive heat, (C) — ohmic heat.

Deleted: 15

Deleted: 13

For Peer Review

1		
2		
3	Page 29: [1] Formatted	4/7/2010 11:07:00 AM
4	Font: 12 pt	
5		
6	Page 29: [1] Formatted	4/7/2010 11:07:00 AM
7	Font: 12 pt, <i>Italic</i>	
8		
9	Page 29: [1] Formatted	4/7/2010 11:07:00 AM
10	Font: 12 pt	
11	Page 29: [1] Formatted	4/7/2010 11:07:00 AM
12	Font: 12 pt, Bold	
13		
14	Page 29: [1] Formatted	4/7/2010 11:07:00 AM
15	Font: 12 pt	
16		
17	Page 29: [1] Formatted	4/7/2010 11:07:00 AM
18	Font: 12 pt, <i>Italic</i>	
19	Page 29: [1] Formatted	4/7/2010 11:07:00 AM
20	Font: 12 pt	
21		
22	Page 29: [2] Formatted	4/7/2010 11:07:00 AM
23	Font: 12 pt, <i>Italic</i>	
24	Page 29: [2] Formatted	4/7/2010 11:07:00 AM
25	Font: 12 pt	
26		
27	Page 29: [2] Formatted	4/7/2010 11:07:00 AM
28	Font: 12 pt, Bold	
29	Page 29: [2] Formatted	4/7/2010 11:07:00 AM
30	Font: 12 pt	
31		
32	Page 29: [2] Formatted	4/7/2010 11:07:00 AM
33	Font: 12 pt, <i>Italic</i>	
34	Page 29: [2] Formatted	4/7/2010 11:07:00 AM
35	Font: 12 pt	
36		
37	Page 29: [3] Formatted	4/7/2010 11:07:00 AM
38	Font: 12 pt, <i>Italic</i>	
39	Page 29: [3] Formatted	4/7/2010 11:07:00 AM
40	Font: 12 pt	
41		
42	Page 29: [3] Formatted	4/7/2010 11:07:00 AM
43	Font: 12 pt, Bold	
44	Page 29: [3] Formatted	4/7/2010 11:07:00 AM
45	Font: 12 pt	
46		
47	Page 29: [3] Formatted	4/7/2010 11:07:00 AM
48	Font: 12 pt, <i>Italic</i>	
49	Page 29: [3] Formatted	4/7/2010 11:07:00 AM
50	Font: 12 pt	
51		
52	Page 29: [4] Formatted	4/7/2010 11:07:00 AM
53	Font: 12 pt, <i>Italic</i>	
54	Page 29: [4] Formatted	4/7/2010 11:07:00 AM
55	Font: 12 pt	
56		
57	Page 29: [4] Formatted	4/7/2010 11:07:00 AM
58	Font: 12 pt	
59		
60		

1
2
3
4
5
6
7
8
9
10
11
12
13
14
15
16
17
18
19
20
21
22
23
24
25
26
27
28
29
30
31
32
33
34
35
36
37
38
39
40
41
42
43
44
45
46
47
48
49
50
51
52
53
54
55
56
57
58
59
60

Page 29: [4] Formatted Font: 12 pt, Bold	4/7/2010 11:07:00 AM
Page 29: [4] Formatted Font: 12 pt	4/7/2010 11:07:00 AM
Page 29: [4] Formatted Font: 12 pt, Italic	4/7/2010 11:07:00 AM
Page 29: [4] Formatted Font: 12 pt	4/7/2010 11:07:00 AM
Page 29: [5] Formatted Font: 12 pt, Italic	4/7/2010 11:07:00 AM
Page 29: [5] Formatted Font: 12 pt	4/7/2010 11:07:00 AM
Page 29: [5] Formatted Font: 12 pt, Bold	4/7/2010 11:07:00 AM
Page 29: [5] Formatted Font: 12 pt	4/7/2010 11:07:00 AM
Page 29: [5] Formatted Font: 12 pt, Italic	4/7/2010 11:07:00 AM
Page 29: [5] Formatted Font: 12 pt	4/7/2010 11:07:00 AM
Page 29: [6] Formatted Font: 12 pt, Italic	4/7/2010 11:07:00 AM
Page 29: [6] Formatted Font: 12 pt	4/7/2010 11:07:00 AM
Page 29: [6] Formatted Font: 12 pt, Bold	4/7/2010 11:07:00 AM
Page 29: [6] Formatted Font: 12 pt	4/7/2010 11:07:00 AM
Page 29: [6] Formatted Font: 12 pt, Italic	4/7/2010 11:07:00 AM
Page 29: [6] Formatted Font: 12 pt	4/7/2010 11:07:00 AM
Page 29: [7] Formatted Font: 12 pt, Italic	4/7/2010 11:07:00 AM
Page 29: [7] Formatted Font: 12 pt	4/7/2010 11:07:00 AM
Page 29: [7] Formatted Font: 12 pt, Bold	4/7/2010 11:07:00 AM
Page 29: [7] Formatted Font: 12 pt	4/7/2010 11:07:00 AM
Page 29: [7] Formatted Font: 12 pt, Italic	4/7/2010 11:07:00 AM

1		
2		
3	Page 29: [7] Formatted	4/7/2010 11:07:00 AM
4	Font: 12 pt	
5		
6	Page 29: [8] Formatted	4/7/2010 11:07:00 AM
7	Font: 12 pt, Italic	
8		
9	Page 29: [8] Formatted	4/7/2010 11:07:00 AM
10	Font: 12 pt	
11		
12	Page 29: [8] Formatted	4/7/2010 11:07:00 AM
13	Font: 12 pt, Bold	
14		
15	Page 29: [8] Formatted	4/7/2010 11:07:00 AM
16	Font: 12 pt	
17		
18	Page 29: [8] Formatted	4/7/2010 11:07:00 AM
19	Font: 12 pt, Italic	
20		
21	Page 29: [8] Formatted	4/7/2010 11:07:00 AM
22	Font: 12 pt	
23		
24	Page 29: [9] Formatted	4/7/2010 11:07:00 AM
25	Font: 12 pt, Italic	
26		
27	Page 29: [9] Formatted	4/7/2010 11:07:00 AM
28	Font: 12 pt, Bold	
29		
30	Page 29: [9] Formatted	4/7/2010 11:07:00 AM
31	Font: 12 pt	
32		
33	Page 29: [9] Formatted	4/7/2010 11:07:00 AM
34	Font: 12 pt, Italic	
35		
36	Page 29: [9] Formatted	4/7/2010 11:07:00 AM
37	Font: 12 pt	
38		
39	Page 29: [10] Formatted	4/7/2010 11:07:00 AM
40	Font: 12 pt, Italic	
41		
42	Page 29: [10] Formatted	4/7/2010 11:07:00 AM
43	Font: 12 pt	
44		
45	Page 29: [10] Formatted	4/7/2010 11:07:00 AM
46	Font: 12 pt, Bold	
47		
48	Page 29: [10] Formatted	4/7/2010 11:07:00 AM
49	Font: 12 pt, Italic	
50		
51	Page 29: [10] Formatted	4/7/2010 11:07:00 AM
52	Font: 12 pt	
53		
54	Page 29: [11] Formatted	4/7/2010 11:07:00 AM
55	Font: 12 pt, Italic	
56		
57	Page 29: [11] Formatted	4/7/2010 11:07:00 AM
58	Font: 12 pt, Italic, Portuguese Portugal	
59		
60		

1		
2		
3	Page 29: [11] Formatted	4/7/2010 11:07:00 AM
4	Font: 12 pt, Portuguese Portugal	
5		
6	Page 29: [11] Formatted	4/7/2010 11:07:00 AM
7	Font: 12 pt, Bold, Portuguese Portugal	
8		
9	Page 29: [11] Formatted	4/7/2010 11:07:00 AM
10	Font: 12 pt, Portuguese Portugal	
11	Page 29: [11] Formatted	4/7/2010 11:07:00 AM
12	Font: 12 pt, Italic, Portuguese Portugal	
13		
14	Page 29: [11] Formatted	4/7/2010 11:07:00 AM
15	Font: 12 pt, Portuguese Portugal	
16		
17	Page 29: [12] Formatted	4/7/2010 11:07:00 AM
18	Font: 12 pt, Italic, Portuguese Portugal	
19		
20	Page 29: [12] Formatted	4/7/2010 11:07:00 AM
21	Font: 12 pt, Italic	
22	Page 29: [12] Formatted	4/7/2010 11:07:00 AM
23	Font: 12 pt	
24	Page 29: [12] Formatted	4/7/2010 11:07:00 AM
25	Font: 12 pt, Bold	
26		
27	Page 29: [12] Formatted	4/7/2010 11:07:00 AM
28	Font: 12 pt	
29		
30	Page 29: [12] Formatted	4/7/2010 11:07:00 AM
31	Font: 12 pt, Italic	
32	Page 29: [12] Formatted	4/7/2010 11:07:00 AM
33	Font: 12 pt	
34		
35	Page 29: [13] Formatted	4/7/2010 11:07:00 AM
36	Font: 12 pt, Italic	
37	Page 29: [13] Formatted	4/7/2010 11:07:00 AM
38	Font: 12 pt	
39		
40	Page 29: [13] Formatted	4/7/2010 11:07:00 AM
41	Font: 12 pt, Bold	
42		
43	Page 29: [13] Formatted	4/7/2010 11:07:00 AM
44	Font: 12 pt	
45	Page 29: [13] Formatted	4/7/2010 11:07:00 AM
46	Font: 12 pt, Italic	
47		
48	Page 29: [13] Formatted	4/7/2010 11:07:00 AM
49	Font: 12 pt	
50		
51	Page 29: [14] Formatted	4/7/2010 11:07:00 AM
52	Font: 12 pt, Italic	
53	Page 29: [14] Formatted	4/7/2010 11:07:00 AM
54	Font: 12 pt	
55		
56	Page 29: [14] Formatted	4/7/2010 11:07:00 AM
57	Font: 12 pt, Bold	
58		
59		
60		

1		
2		
3	Page 29: [14] Formatted	4/7/2010 11:07:00 AM
4	Font: 12 pt	
5		
6	Page 29: [14] Formatted	4/7/2010 11:07:00 AM
7	Font: 12 pt, <i>Italic</i>	
8		
9	Page 29: [14] Formatted	4/7/2010 11:07:00 AM
10	Font: 12 pt	
11	Page 29: [15] Formatted	4/7/2010 11:07:00 AM
12	Font: 12 pt, <i>Italic</i>	
13		
14	Page 29: [15] Formatted	4/7/2010 11:07:00 AM
15	Font: 12 pt	
16		
17	Page 29: [15] Formatted	4/7/2010 11:07:00 AM
18	Font: 12 pt, Bold	
19		
20	Page 29: [15] Formatted	4/7/2010 11:07:00 AM
21	Font: 12 pt	
22	Page 29: [15] Formatted	4/7/2010 11:07:00 AM
23	Font: 12 pt, <i>Italic</i>	
24		
25	Page 29: [15] Formatted	4/7/2010 11:07:00 AM
26	Font: 12 pt	
27	Page 29: [16] Formatted	4/7/2010 11:07:00 AM
28	Font: 12 pt, <i>Italic</i>	
29		
30	Page 29: [16] Formatted	4/7/2010 11:07:00 AM
31	Font: 12 pt	
32	Page 29: [16] Formatted	4/7/2010 11:07:00 AM
33	Font: 12 pt, Bold	
34		
35	Page 29: [16] Formatted	4/7/2010 11:07:00 AM
36	Font: 12 pt	
37	Page 29: [16] Formatted	4/7/2010 11:07:00 AM
38	Font: 12 pt, <i>Italic</i>	
39		
40	Page 29: [16] Formatted	4/7/2010 11:07:00 AM
41	Font: 12 pt	
42		
43	Page 29: [17] Formatted	4/7/2010 11:07:00 AM
44	Font: 12 pt, <i>Italic</i>	
45		
46	Page 29: [17] Formatted	4/7/2010 11:07:00 AM
47	Font: 12 pt	
48	Page 29: [17] Formatted	4/7/2010 11:07:00 AM
49	Font: 12 pt, Bold	
50		
51	Page 29: [17] Formatted	4/7/2010 11:07:00 AM
52	Font: 12 pt	
53	Page 29: [17] Formatted	4/7/2010 11:07:00 AM
54	Font: 12 pt, <i>Italic</i>	
55		
56	Page 29: [17] Formatted	4/7/2010 11:07:00 AM
57	Font: 12 pt	
58		
59		
60		

1		
2		
3	Page 29: [18] Formatted	4/7/2010 11:07:00 AM
4	Font: 12 pt, <i>Italic</i>	
5		
6	Page 29: [18] Formatted	4/7/2010 11:07:00 AM
7	Font: 12 pt	
8		
9	Page 29: [18] Formatted	4/7/2010 11:07:00 AM
10	Font: 12 pt, Bold	
11	Page 29: [18] Formatted	4/7/2010 11:07:00 AM
12	Font: 12 pt	
13		
14	Page 29: [18] Formatted	4/7/2010 11:07:00 AM
15	Font: 12 pt, <i>Italic</i>	
16		
17	Page 29: [18] Formatted	4/7/2010 11:07:00 AM
18	Font: 12 pt	
19	Page 29: [19] Formatted	4/7/2010 11:07:00 AM
20	Font: 12 pt, <i>Italic</i>	
21		
22	Page 29: [19] Formatted	4/7/2010 11:07:00 AM
23	Font: 12 pt	
24	Page 29: [19] Formatted	4/7/2010 11:07:00 AM
25	Font: 12 pt, Bold	
26		
27	Page 29: [19] Formatted	4/7/2010 11:07:00 AM
28	Font: 12 pt	
29		
30	Page 29: [19] Formatted	4/7/2010 11:07:00 AM
31	Font: 12 pt, <i>Italic</i>	
32	Page 29: [19] Formatted	4/7/2010 11:07:00 AM
33	Font: 12 pt	
34		
35	Page 29: [20] Formatted	4/7/2010 11:07:00 AM
36	Font: 12 pt, <i>Italic</i>	
37	Page 29: [20] Formatted	4/7/2010 11:07:00 AM
38	Font: 12 pt	
39		
40	Page 29: [20] Formatted	4/7/2010 11:07:00 AM
41	Font: 12 pt, Bold	
42		
43	Page 29: [20] Formatted	4/7/2010 11:07:00 AM
44	Font: 12 pt	
45	Page 29: [20] Formatted	4/7/2010 11:07:00 AM
46	Font: 12 pt, <i>Italic</i>	
47		
48	Page 29: [20] Formatted	4/7/2010 11:07:00 AM
49	Font: 12 pt	
50		
51	Page 29: [21] Formatted	4/7/2010 11:07:00 AM
52	Font: 12 pt, <i>Italic</i>	
53	Page 29: [21] Formatted	4/7/2010 11:07:00 AM
54	Font: 12 pt	
55		
56	Page 29: [21] Formatted	4/7/2010 11:07:00 AM
57	Font: 12 pt, Bold	
58		
59		
60		

1		
2		
3	Page 29: [21] Formatted	4/7/2010 11:07:00 AM
4	Font: 12 pt	
5		
6	Page 29: [21] Formatted	4/7/2010 11:07:00 AM
7	Font: 12 pt, <i>Italic</i>	
8		
9	Page 29: [21] Formatted	4/7/2010 11:07:00 AM
10	Font: 12 pt	
11	Page 29: [22] Formatted	4/7/2010 11:07:00 AM
12	Font: 12 pt, <i>Italic</i>	
13		
14	Page 29: [22] Formatted	4/7/2010 11:07:00 AM
15	Font: 12 pt	
16		
17	Page 29: [22] Formatted	4/7/2010 11:07:00 AM
18	Font: 12 pt, Bold	
19		
20	Page 29: [22] Formatted	4/7/2010 11:07:00 AM
21	Font: 12 pt	
22	Page 29: [22] Formatted	4/7/2010 11:07:00 AM
23	Font: 12 pt, <i>Italic</i>	
24		
25	Page 29: [22] Formatted	4/7/2010 11:07:00 AM
26	Font: 12 pt	
27	Page 29: [23] Formatted	4/7/2010 11:07:00 AM
28	Font: 12 pt, <i>Italic</i>	
29		
30	Page 29: [23] Formatted	4/7/2010 11:07:00 AM
31	Font: 12 pt	
32	Page 29: [23] Formatted	4/7/2010 11:07:00 AM
33	Font: 12 pt, Bold	
34		
35	Page 29: [23] Formatted	4/7/2010 11:07:00 AM
36	Font: 12 pt	
37	Page 29: [23] Formatted	4/7/2010 11:07:00 AM
38	Font: 12 pt, <i>Italic</i>	
39		
40	Page 29: [23] Formatted	4/7/2010 11:07:00 AM
41	Font: 12 pt	
42		
43	Page 29: [24] Formatted	4/7/2010 11:07:00 AM
44	Font: 12 pt, <i>Italic</i>	
45		
46	Page 29: [24] Formatted	4/7/2010 11:07:00 AM
47	Font: 12 pt	
48	Page 29: [24] Formatted	4/7/2010 11:07:00 AM
49	Font: 12 pt, Bold	
50		
51	Page 29: [24] Formatted	4/7/2010 11:07:00 AM
52	Font: 12 pt	
53	Page 29: [24] Formatted	4/7/2010 11:07:00 AM
54	Font: 12 pt, <i>Italic</i>	
55		
56	Page 29: [24] Formatted	4/7/2010 11:07:00 AM
57	Font: 12 pt	
58		
59		
60		

1		
2		
3	Page 29: [25] Formatted	4/7/2010 11:07:00 AM
4	Font: 12 pt, <i>Italic</i>	
5		
6	Page 29: [25] Formatted	4/7/2010 11:07:00 AM
7	Font: 12 pt	
8		
9	Page 29: [25] Formatted	4/7/2010 11:07:00 AM
10	Font: 12 pt, Bold	
11		
12	Page 29: [25] Formatted	4/7/2010 11:07:00 AM
13	Font: 12 pt	
14		
15	Page 29: [25] Formatted	4/7/2010 11:07:00 AM
16	Font: 12 pt, <i>Italic</i>	
17		
18	Page 29: [25] Formatted	4/7/2010 11:07:00 AM
19	Font: 12 pt	
20		
21	Page 29: [26] Formatted	4/7/2010 11:07:00 AM
22	Font: 12 pt, <i>Italic</i>	
23		
24	Page 29: [26] Formatted	4/7/2010 11:07:00 AM
25	Font: 12 pt	
26		
27	Page 29: [26] Formatted	4/7/2010 11:07:00 AM
28	Font: 12 pt, Bold	
29		
30	Page 29: [26] Formatted	4/7/2010 11:07:00 AM
31	Font: 12 pt, <i>Italic</i>	
32		
33	Page 29: [26] Formatted	4/7/2010 11:07:00 AM
34	Font: 12 pt	
35		
36	Page 29: [27] Formatted	4/7/2010 11:07:00 AM
37	Font: 12 pt, <i>Italic</i>	
38		
39	Page 29: [27] Formatted	4/7/2010 11:07:00 AM
40	Font: 12 pt	
41		
42	Page 29: [27] Formatted	4/7/2010 11:07:00 AM
43	Font: 12 pt, Bold	
44		
45	Page 29: [27] Formatted	4/7/2010 11:07:00 AM
46	Font: 12 pt	
47		
48	Page 29: [27] Formatted	4/7/2010 11:07:00 AM
49	Font: 12 pt, <i>Italic</i>	
50		
51	Page 29: [27] Formatted	4/7/2010 11:07:00 AM
52	Font: 12 pt	
53		
54	Page 29: [28] Formatted	4/7/2010 11:07:00 AM
55	Font: 12 pt, <i>Italic</i>	
56		
57	Page 29: [28] Formatted	4/7/2010 11:07:00 AM
58	Font: 12 pt, Bold	
59		
60		

1		
2		
3	Page 29: [28] Formatted	4/7/2010 11:07:00 AM
4	Font: 12 pt	
5		
6	Page 29: [28] Formatted	4/7/2010 11:07:00 AM
7	Font: 12 pt, <i>Italic</i>	
8		
9	Page 29: [28] Formatted	4/7/2010 11:07:00 AM
10	Font: 12 pt	
11	Page 29: [29] Formatted	4/7/2010 11:07:00 AM
12	Font: 12 pt, <i>Italic</i>	
13		
14	Page 29: [29] Formatted	4/7/2010 11:07:00 AM
15	Font: 12 pt	
16		
17	Page 29: [29] Formatted	4/7/2010 11:07:00 AM
18	Font: 12 pt, <i>Italic</i>	
19		
20	Page 29: [29] Formatted	4/7/2010 11:07:00 AM
21	Font: 12 pt	
22	Page 29: [30] Formatted	4/7/2010 11:07:00 AM
23	Font: 12 pt, <i>Italic</i>	
24		
25	Page 29: [30] Formatted	4/7/2010 11:07:00 AM
26	Font: 12 pt	
27	Page 29: [30] Formatted	4/7/2010 11:07:00 AM
28	Font: 12 pt, Bold	
29		
30	Page 29: [30] Formatted	4/7/2010 11:07:00 AM
31	Font: 12 pt	
32	Page 29: [30] Formatted	4/7/2010 11:07:00 AM
33	Font: 12 pt, <i>Italic</i>	
34		
35	Page 29: [30] Formatted	4/7/2010 11:07:00 AM
36	Font: 12 pt	
37	Page 29: [31] Formatted	4/7/2010 11:07:00 AM
38	Font: 12 pt, <i>Italic</i>	
39		
40	Page 29: [31] Formatted	4/7/2010 11:07:00 AM
41	Font: 12 pt	
42		
43	Page 29: [31] Formatted	4/7/2010 11:07:00 AM
44	Font: 12 pt, Bold	
45		
46	Page 29: [31] Formatted	4/7/2010 11:07:00 AM
47	Font: 12 pt	
48	Page 29: [31] Formatted	4/7/2010 11:07:00 AM
49	Font: 12 pt, <i>Italic</i>	
50		
51	Page 29: [31] Formatted	4/7/2010 11:07:00 AM
52	Font: 12 pt	
53	Page 29: [32] Formatted	4/7/2010 11:07:00 AM
54	Font: 12 pt, <i>Italic</i>	
55		
56	Page 29: [32] Formatted	4/7/2010 11:07:00 AM
57	Font: 12 pt	
58		
59		
60		

1
2
3
4
5
6
7
8
9
10
11
12
13
14
15
16
17
18
19
20
21
22
23
24
25
26
27
28
29
30
31
32
33
34
35
36
37
38
39
40
41
42
43
44
45
46
47
48
49
50
51
52
53
54
55
56
57
58
59
60

Page 29: [32] Formatted	4/7/2010 11:07:00 AM
Font: 12 pt, Bold	
Page 29: [32] Formatted	4/7/2010 11:07:00 AM
Font: 12 pt	
Page 29: [32] Formatted	4/7/2010 11:07:00 AM
Font: 12 pt, Italic	
Page 29: [32] Formatted	4/7/2010 11:07:00 AM
Font: 12 pt	
Page 29: [33] Formatted	4/7/2010 11:07:00 AM
Font: 12 pt, Italic	
Page 29: [33] Formatted	4/7/2010 11:07:00 AM
Font: 12 pt	
Page 29: [33] Formatted	4/7/2010 11:07:00 AM
Font: 12 pt, Bold	
Page 29: [33] Formatted	4/7/2010 11:07:00 AM
Font: 12 pt	
Page 29: [34] Formatted	4/7/2010 11:07:00 AM
Font: 12 pt, Italic	
Page 29: [34] Formatted	4/7/2010 11:07:00 AM
Font: 12 pt	
Page 29: [34] Formatted	4/7/2010 11:07:00 AM
Font: 12 pt, Italic	
Page 29: [34] Formatted	4/7/2010 11:07:00 AM
Font: 12 pt	
Page 29: [35] Formatted	4/7/2010 11:07:00 AM
Font: 12 pt, Italic	
Page 29: [35] Formatted	4/7/2010 11:07:00 AM
Font: 12 pt	
Page 29: [35] Formatted	4/7/2010 11:07:00 AM
Font: 12 pt, Bold	
Page 29: [35] Formatted	4/7/2010 11:07:00 AM
Font: 12 pt	
Page 29: [35] Formatted	4/7/2010 11:07:00 AM
Font: 12 pt, Italic	
Page 29: [35] Formatted	4/7/2010 11:07:00 AM
Font: 12 pt	
Page 29: [36] Formatted	4/7/2010 11:07:00 AM
Font: 12 pt, Italic	
Page 29: [36] Formatted	4/7/2010 11:07:00 AM
Font: 12 pt	
Page 29: [36] Formatted	4/7/2010 11:07:00 AM
Font: 12 pt, Bold	

1		
2		
3	Page 29: [36] Formatted	4/7/2010 11:07:00 AM
4	Font: 12 pt	
5		
6	Page 29: [36] Formatted	4/7/2010 11:07:00 AM
7	Font: 12 pt, <i>Italic</i>	
8		
9	Page 29: [36] Formatted	4/7/2010 11:07:00 AM
10	Font: 12 pt	
11	Page 29: [37] Formatted	4/7/2010 11:07:00 AM
12	Font: 12 pt, <i>Italic</i>	
13		
14	Page 29: [37] Formatted	4/7/2010 11:07:00 AM
15	Font: 12 pt	
16		
17	Page 29: [37] Formatted	4/7/2010 11:07:00 AM
18	Font: 12 pt, Bold	
19		
20	Page 29: [37] Formatted	4/7/2010 11:07:00 AM
21	Font: 12 pt	
22	Page 29: [37] Formatted	4/7/2010 11:07:00 AM
23	Font: 12 pt, <i>Italic</i>	
24		
25	Page 29: [37] Formatted	4/7/2010 11:07:00 AM
26	Font: 12 pt	
27	Page 29: [38] Formatted	4/7/2010 11:07:00 AM
28	Font: 12 pt, <i>Italic</i>	
29		
30	Page 29: [38] Formatted	4/7/2010 11:07:00 AM
31	Font: 12 pt	
32	Page 29: [38] Formatted	4/7/2010 11:07:00 AM
33	Font: 12 pt, Bold	
34		
35	Page 29: [38] Formatted	4/7/2010 11:07:00 AM
36	Font: 12 pt	
37	Page 29: [38] Formatted	4/7/2010 11:07:00 AM
38	Font: 12 pt, <i>Italic</i>	
39		
40	Page 29: [38] Formatted	4/7/2010 11:07:00 AM
41	Font: 12 pt	
42		
43	Page 29: [39] Formatted	4/7/2010 11:07:00 AM
44	Hyperlink, Font: 12 pt	
45		
46	Page 29: [39] Formatted	4/7/2010 11:07:00 AM
47	Font: 12 pt	
48	Page 29: [40] Formatted	4/7/2010 11:07:00 AM
49	Font: 12 pt, <i>Italic</i>	
50		
51	Page 29: [40] Formatted	4/7/2010 11:07:00 AM
52	Font: 12 pt	
53	Page 29: [40] Formatted	4/7/2010 11:07:00 AM
54	Font: 12 pt, Bold	
55		
56	Page 29: [40] Formatted	4/7/2010 11:07:00 AM
57	Font: 12 pt	
58		
59		
60		

1
2
3
4
5
6
7
8
9
10
11
12
13
14
15
16
17
18
19
20
21
22
23
24
25
26
27
28
29
30
31
32
33
34
35
36
37
38
39
40
41
42
43
44
45
46
47
48
49
50
51
52
53
54
55
56
57
58
59
60

Page 29: [40] Formatted	4/7/2010 11:07:00 AM
Font: 12 pt, <i>Italic</i>	
Page 29: [40] Formatted	4/7/2010 11:07:00 AM
Font: 12 pt	
Page 30: [41] Formatted	4/7/2010 11:07:00 AM
Font: 12 pt, <i>Italic</i>	
Page 30: [41] Formatted	4/7/2010 11:07:00 AM
Font: 12 pt	
Page 30: [41] Formatted	4/7/2010 11:07:00 AM
Font: 12 pt, Bold	
Page 30: [41] Formatted	4/7/2010 11:07:00 AM
Font: 12 pt	
Page 30: [41] Formatted	4/7/2010 11:07:00 AM
Font: 12 pt, <i>Italic</i>	
Page 30: [41] Formatted	4/7/2010 11:07:00 AM
Font: 12 pt	
Page 30: [42] Formatted	4/7/2010 11:07:00 AM
Font: 12 pt, <i>Italic</i>	
Page 30: [42] Formatted	4/7/2010 11:07:00 AM
Font: 12 pt	
Page 30: [42] Formatted	4/7/2010 11:07:00 AM
Font: 12 pt, Bold	
Page 30: [42] Formatted	4/7/2010 11:07:00 AM
Font: 12 pt	
Page 30: [42] Formatted	4/7/2010 11:07:00 AM
Font: 12 pt, <i>Italic</i>	
Page 30: [42] Formatted	4/7/2010 11:07:00 AM
Font: 12 pt	
Page 30: [43] Formatted	4/7/2010 11:07:00 AM
Hyperlink, Font: 12 pt	
Page 30: [43] Formatted	4/7/2010 11:07:00 AM
Font: 12 pt	
Page 30: [44] Formatted	4/7/2010 11:07:00 AM
Hyperlink, Font: 12 pt	
Page 30: [44] Formatted	4/7/2010 11:07:00 AM
Font: 12 pt	
Page 30: [45] Formatted	4/7/2010 11:07:00 AM
Font: 12 pt, <i>Italic</i>	
Page 30: [45] Formatted	4/7/2010 11:07:00 AM
Font: 12 pt	
Page 30: [45] Formatted	4/7/2010 11:07:00 AM
Font: 12 pt, Bold	

1		
2		
3	Page 30: [45] Formatted	4/7/2010 11:07:00 AM
4	Font: 12 pt	
5		
6	Page 30: [45] Formatted	4/7/2010 11:07:00 AM
7	Font: 12 pt, <i>Italic</i>	
8		
9	Page 30: [45] Formatted	4/7/2010 11:07:00 AM
10	Font: 12 pt	
11	Page 30: [46] Formatted	4/7/2010 11:07:00 AM
12	Font: 12 pt, <i>Italic</i>	
13		
14	Page 30: [46] Formatted	4/7/2010 11:07:00 AM
15	Font: 12 pt	
16		
17	Page 30: [46] Formatted	4/7/2010 11:07:00 AM
18	Font: 12 pt, Bold	
19		
20	Page 30: [46] Formatted	4/7/2010 11:07:00 AM
21	Font: 12 pt	
22	Page 30: [47] Formatted	4/7/2010 11:07:00 AM
23	Font: 12 pt, <i>Italic</i>	
24		
25	Page 30: [47] Formatted	4/7/2010 11:07:00 AM
26	Font: 12 pt	
27	Page 30: [47] Formatted	4/7/2010 11:07:00 AM
28	Font: 12 pt, Bold	
29		
30	Page 30: [47] Formatted	4/7/2010 11:07:00 AM
31	Font: 12 pt	
32	Page 30: [48] Formatted	4/7/2010 11:07:00 AM
33	Font: 12 pt, <i>Italic</i>	
34		
35	Page 30: [48] Formatted	4/7/2010 11:07:00 AM
36	Font: 12 pt	
37	Page 30: [48] Formatted	4/7/2010 11:07:00 AM
38	Font: 12 pt, Bold	
39		
40	Page 30: [48] Formatted	4/7/2010 11:07:00 AM
41	Font: 12 pt	
42		
43	Page 30: [48] Formatted	4/7/2010 11:07:00 AM
44	Font: 12 pt, <i>Italic</i>	
45		
46	Page 30: [48] Formatted	4/7/2010 11:07:00 AM
47	Font: 12 pt	
48	Page 30: [49] Formatted	4/7/2010 11:07:00 AM
49	Hyperlink, Font: 12 pt	
50		
51	Page 30: [49] Formatted	4/7/2010 11:07:00 AM
52	Font: 12 pt	
53	Page 30: [50] Formatted	4/7/2010 11:07:00 AM
54	Hyperlink, Font: 12 pt	
55		
56	Page 30: [50] Formatted	4/7/2010 11:07:00 AM
57	Font: 12 pt	
58		
59		
60		

1		
2		
3	Page 30: [51] Formatted	4/7/2010 11:07:00 AM
4	Font: 12 pt, <i>Italic</i>	
5		
6	Page 30: [51] Formatted	4/7/2010 11:07:00 AM
7	Font: 12 pt	
8		
9	Page 30: [51] Formatted	4/7/2010 11:07:00 AM
10	Font: 12 pt, Bold	
11	Page 30: [51] Formatted	4/7/2010 11:07:00 AM
12	Font: 12 pt	
13		
14	Page 30: [51] Formatted	4/7/2010 11:07:00 AM
15	Font: 12 pt, <i>Italic</i>	
16		
17	Page 30: [51] Formatted	4/7/2010 11:07:00 AM
18	Font: 12 pt	
19	Page 30: [52] Formatted	4/7/2010 11:07:00 AM
20	Font: 12 pt, <i>Italic</i>	
21		
22	Page 30: [52] Formatted	4/7/2010 11:07:00 AM
23	Font: 12 pt	
24	Page 30: [52] Formatted	4/7/2010 11:07:00 AM
25	Font: 12 pt, Bold	
26		
27	Page 30: [52] Formatted	4/7/2010 11:07:00 AM
28	Font: 12 pt	
29		
30	Page 30: [52] Formatted	4/7/2010 11:07:00 AM
31	Font: 12 pt, <i>Italic</i>	
32	Page 30: [52] Formatted	4/7/2010 11:07:00 AM
33	Font: 12 pt	
34		
35	Page 30: [53] Formatted	4/7/2010 11:07:00 AM
36	Font: 12 pt, <i>Italic</i>	
37	Page 30: [53] Formatted	4/7/2010 11:07:00 AM
38	Font: 12 pt	
39		
40	Page 30: [53] Formatted	4/7/2010 11:07:00 AM
41	Font: 12 pt, Bold	
42		
43	Page 30: [53] Formatted	4/7/2010 11:07:00 AM
44	Font: 12 pt	
45	Page 30: [53] Formatted	4/7/2010 11:07:00 AM
46	Font: 12 pt, <i>Italic</i>	
47		
48	Page 30: [53] Formatted	4/7/2010 11:07:00 AM
49	Font: 12 pt	
50		
51	Page 30: [54] Formatted	4/7/2010 11:07:00 AM
52	Font: 12 pt, <i>Italic</i>	
53	Page 30: [54] Formatted	4/7/2010 11:07:00 AM
54	Font: 12 pt	
55		
56	Page 30: [54] Formatted	4/7/2010 11:07:00 AM
57	Font: 12 pt, Bold	
58		
59		
60		

1		
2		
3	Page 30: [54] Formatted	4/7/2010 11:07:00 AM
4	Font: 12 pt	
5		
6	Page 30: [54] Formatted	4/7/2010 11:07:00 AM
7	Font: 12 pt, <i>Italic</i>	
8		
9	Page 30: [54] Formatted	4/7/2010 11:07:00 AM
10	Font: 12 pt	
11	Page 30: [55] Formatted	4/7/2010 11:07:00 AM
12	Font: 12 pt, <i>Italic</i>	
13		
14	Page 30: [55] Formatted	4/7/2010 11:07:00 AM
15	Font: 12 pt	
16		
17	Page 30: [55] Formatted	4/7/2010 11:07:00 AM
18	Font: 12 pt, Bold	
19		
20	Page 30: [55] Formatted	4/7/2010 11:07:00 AM
21	Font: 12 pt	
22	Page 30: [55] Formatted	4/7/2010 11:07:00 AM
23	Font: 12 pt, <i>Italic</i>	
24		
25	Page 30: [55] Formatted	4/7/2010 11:07:00 AM
26	Font: 12 pt	
27	Page 30: [56] Formatted	4/7/2010 11:07:00 AM
28	Font: 12 pt, <i>Italic</i>	
29		
30	Page 30: [56] Formatted	4/7/2010 11:07:00 AM
31	Font: 12 pt	
32	Page 30: [56] Formatted	4/7/2010 11:07:00 AM
33	Font: 12 pt, Bold	
34		
35	Page 30: [56] Formatted	4/7/2010 11:07:00 AM
36	Font: 12 pt	
37	Page 30: [56] Formatted	4/7/2010 11:07:00 AM
38	Font: 12 pt, <i>Italic</i>	
39		
40	Page 30: [56] Formatted	4/7/2010 11:07:00 AM
41	Font: 12 pt	
42		
43	Page 30: [57] Formatted	4/7/2010 11:07:00 AM
44	Font: 12 pt, <i>Italic</i>	
45		
46	Page 30: [57] Formatted	4/7/2010 11:07:00 AM
47	Font: 12 pt	
48	Page 30: [57] Formatted	4/7/2010 11:07:00 AM
49	Font: 12 pt, Bold	
50		
51	Page 30: [57] Formatted	4/7/2010 11:07:00 AM
52	Font: 12 pt	
53	Page 30: [57] Formatted	4/7/2010 11:07:00 AM
54	Font: 12 pt, <i>Italic</i>	
55		
56	Page 30: [57] Formatted	4/7/2010 11:07:00 AM
57	Font: 12 pt	
58		
59		
60		

1		
2		
3	Page 30: [58] Formatted	4/7/2010 11:07:00 AM
4	Font: 12 pt, <i>Italic</i>	
5		
6	Page 30: [58] Formatted	4/7/2010 11:07:00 AM
7	Font: 12 pt	
8		
9	Page 30: [58] Formatted	4/7/2010 11:07:00 AM
10	Font: 12 pt, Bold	
11	Page 30: [58] Formatted	4/7/2010 11:07:00 AM
12	Font: 12 pt	
13		
14	Page 30: [59] Formatted	4/7/2010 11:07:00 AM
15	Font: 12 pt, <i>Italic</i>	
16		
17	Page 30: [59] Formatted	4/7/2010 11:07:00 AM
18	Font: 12 pt	
19		
20	Page 30: [59] Formatted	4/7/2010 11:07:00 AM
21	Font: 12 pt, Bold	
22	Page 30: [59] Formatted	4/7/2010 11:07:00 AM
23	Font: 12 pt	
24		
25	Page 30: [60] Formatted	4/7/2010 11:07:00 AM
26	Font: 12 pt, <i>Italic</i>	
27		
28	Page 30: [60] Formatted	4/7/2010 11:07:00 AM
29	Font: 12 pt	
30		
31	Page 30: [60] Formatted	4/7/2010 11:07:00 AM
32	Font: 12 pt, Bold	
33	Page 30: [60] Formatted	4/7/2010 11:07:00 AM
34	Font: 12 pt	
35		
36	Page 30: [60] Formatted	4/7/2010 11:07:00 AM
37	Font: 12 pt, <i>Italic</i>	
38		
39	Page 30: [60] Formatted	4/7/2010 11:07:00 AM
40	Font: 12 pt	
41		
42	Page 30: [61] Formatted	4/7/2010 11:07:00 AM
43	Font: 12 pt, <i>Italic</i>	
44		
45	Page 30: [61] Formatted	4/7/2010 11:07:00 AM
46	Font: 12 pt, Bold	
47		
48	Page 30: [61] Formatted	4/7/2010 11:07:00 AM
49	Font: 12 pt	
50		
51	Page 30: [61] Formatted	4/7/2010 11:07:00 AM
52	Font: 12 pt, <i>Italic</i>	
53		
54	Page 30: [61] Formatted	4/7/2010 11:07:00 AM
55	Font: 12 pt	
56		
57	Page 30: [62] Formatted	4/7/2010 11:07:00 AM
58	Font: 12 pt, <i>Italic</i>	
59		
60		

1		
2		
3	Page 30: [62] Formatted	4/7/2010 11:07:00 AM
4	Font: 12 pt	
5		
6	Page 30: [62] Formatted	4/7/2010 11:07:00 AM
7	Font: 12 pt, Bold	
8		
9	Page 30: [62] Formatted	4/7/2010 11:07:00 AM
10	Font: 12 pt	
11	Page 30: [62] Formatted	4/7/2010 11:07:00 AM
12	Font: 12 pt, Italic	
13		
14	Page 30: [62] Formatted	4/7/2010 11:07:00 AM
15	Font: 12 pt	
16		
17	Page 30: [63] Formatted	4/7/2010 11:07:00 AM
18	Font: 12 pt, Italic	
19	Page 30: [63] Formatted	4/7/2010 11:07:00 AM
20	Font: 12 pt	
21		
22	Page 30: [63] Formatted	4/7/2010 11:07:00 AM
23	Font: 12 pt, Bold	
24	Page 30: [63] Formatted	4/7/2010 11:07:00 AM
25	Font: 12 pt	
26		
27	Page 30: [63] Formatted	4/7/2010 11:07:00 AM
28	Font: 12 pt, Italic	
29	Page 30: [63] Formatted	4/7/2010 11:07:00 AM
30	Font: 12 pt	
31		
32	Page 30: [64] Formatted	4/7/2010 11:07:00 AM
33	Font: 12 pt, Italic	
34	Page 30: [64] Formatted	4/7/2010 11:07:00 AM
35	Font: 12 pt	
36		
37	Page 30: [64] Formatted	4/7/2010 11:07:00 AM
38	Font: 12 pt, Bold	
39	Page 30: [64] Formatted	4/7/2010 11:07:00 AM
40	Font: 12 pt	
41		
42	Page 30: [64] Formatted	4/7/2010 11:07:00 AM
43	Font: 12 pt, Italic	
44	Page 30: [64] Formatted	4/7/2010 11:07:00 AM
45	Font: 12 pt	
46		
47	Page 30: [65] Deleted	3/26/2010 2:50:00 PM
48	[1] J. S. Wainright, J.-T. Wang, D. Weng, R. F. Savinell and M. Litt, <i>J. Electrochem. Soc.</i> 1995, <i>142</i> , L121.	
49	[2] J.-T. Wang, R. F. Savinell, J. Wainright, M. Litt and H. Yu, <i>Electrochim. Acta</i> 1996, <i>41</i> , 593.	
50	[3] S. R. Samms, S. Wasmus and R. F. Savinell, <i>J. Electrochem. Soc.</i> 1996, <i>143</i> , 1225.	
51	[4] Y.-L. Ma, J. S. Wainright, M. H. Litt and R. F. Savinell, <i>J. Electrochem. Soc.</i> 2004, <i>151</i> , A8.	
52	[5] Z. Qi and S. Buelte, <i>J. Power Sources</i> 2006, <i>161</i> , 1126.	
53	[6] P. Jannasch, <i>Curr. Opin. Colloid Interface Sci.</i> 2003, <i>8</i> , 96.	
54		
55		
56		
57		
58		
59		
60		

- 1
2
3 [7] I. Honma, H. Nakajima, O. Nishikawa, T. Sugimoto and S. Nomura, *J. Electrochem. Soc.* 2003, *150*, A616.
- 4 [8] S.-H. Kwak, T.-H. Yang, C.-S. Kim and K. H. Yoon, *Solid State Ionics* 2003, *160*, 309.
- 5 [9] H. Kim, S. An, J. Kim, J. Moon, S. Cho, Y. Eun, H.-K. Yoon, Y. Park, H.-J. Kweon and
6 E.-M. Shin, *Macromol. Rapid Commun.* 2004, *25*, 1410.
- 7 [10] V. Ramani, H. R. Kunz and J. M. Fenton, *J. Membr. Sci.* 2004, *232*, 31.
- 8 [11] S.-H. Kwak, T.-H. Yang, C.-S. Kim and K. H. Yoon, *Electrochim. Acta* 2004, *50*, 653.
- 9 [12] E. K. Pefkianakis, V. Deimede, M. K. Daletou, N. Gourdoupi and J. K. Kallitis,
10 *Macromol. Rapid Commun.* 2005, *26*, 1724.
- 11 [13] J. A. Asensio and P. Gomez-Romero, *Fuel Cells* 2005, *5*, 336.
- 12 [14] L. Xiao, H. Zhang, T. Jana, E. Scanlon, R. Chen, E.-W. Choe, L. S. Ramanathan, S. Yu
13 and B. C. Benicewicz, *Fuel Cells* 2005, *5*, 287.
- 14 [15] V. Baglio, A. D. Blasi, A. S. Arico, V. Antonucci, P. L. Antonucci, C. Trakanprapai, V.
15 Esposito, S. Licocchia and E. Traversa, *J. Electrochem. Soc.* 2005, *152*, A1373.
- 16 [16] L. Paturzo, A. Basile, A. Iulianelli, J. C. Jansen, I. Gatto and E. Passalacqua, *Catal.*
17 *Today* 2005, *104*, 213.
- 18 [17] M. Li, H. Zhang and Z.-G. Shao, *Electrochem. Solid-State Lett.* 2006, *9*, A60.
- 19 [18] D. M. Bernardi and M. W. Verbrugge, *AIChE J.* 1991, *37*, 1151.
- 20 [19] L. Ma, D. B. Ingham, M. Pourkashanian and E. Carcadea, *Journal of Fuel Cell Science*
21 *and Technology* 2005, *2*, 246.
- 22 [20] D. Cheddie and N. Munroe, *Journal of Power Sources* 2005, *147*, 72.
- 23 [21] A. Biyikoglu, *Int. J. Hydrogen Energy* 2005, *30*, 1181.
- 24 [22] A. R. Korsgaard, R. Refshauge, M. P. Nielsen, M. Bang and S. K. KÆ, *J. Power Sources*
25 2006, *162*, 239.
- 26 [23] D. Cheddie and N. Munroe, *Energy Convers. Manage.* 2006, *47*, 1490.
- 27 [24] D. Cheddie and N. Munroe, *J. Power Sources* 2006, *156*, 414.
- 28 [25] D. Cheddie and N. Munroe, *J. Power Sources* 2006, *160*, 215.
- 29 [26] D. Cheddie and N. Munroe, *Int. J. Hydrogen Energy* 2007, *32*, 832.
- 30 [27] K. Scott, S. Pilditch and M. Mamlouk, *J. Appl. Electrochem.* 2007, *37*, 1245.
- 31 [28] K. Broka and P. Ekdunge, *J. Appl. Electrochem.* 1997, *27*, 281.
- 32 [29] Carbon Paper, can be found under <http://www.torayca.com>, 2005.
- 33 [30] J. A. Ochoa-Tapia and S. Whitaker, *Int. J. Heat Mass Transfer* 1995, *38*, 2647.
- 34 [31] H. C. Brinkman, *Appl. Sci. Res.* 1949, *1*, 27.
- 35 [32] M. J. Lampinen and M. Fomino, *J. Electrochem. Soc.* 1993, *140*, 3537.
- 36 [33] F. P. Incropera and F. P. Incropera, *Fundamentals of heat and mass transfer*, John Wiley,
37 Hoboken, NJ, 2007.
- 38 [34] K. Klinedinst, J. A. S. Bett, J. Macdonald and P. Stonehart, *J. Electroanal. Chem.* 1974,
39 *57*, 281.
- 40 [35] D. I. MacDonald and J. R. Boyack, *J. Chem. Eng. Data* 1969, *14*, 380.
- 41 [36] R. Bouchet and E. Siebert, *Solid State Ionics* 1999, *118*, 287.
- 42 [37] Y. L. Ma, J. S. Wainright, M. H. Litt and R. F. Savinell, *J. Electrochem. Soc.* 2004, *151*.
- 43 [38] G. Welsch, R. Boyer and E. W. Collings, *Materials properties handbook: titanium alloys*
44 ASM International 1994.
- 45 [39] J. Brandrup, E. H. Immergut, E. A. Grulke and Knovel (Firm), *Polymer handbook*, Wiley,
46 New York, 1999.
- 47 [40] T. Zhou and H. Liu, *J. Power Sources* 2006, *161*, 444.
- 48 [41] W. Vogel, J. Lundquist, P. Ross and P. Stonehart, *Electrochim. Acta* 1974, *20*, 79.
- 49 [42] J. MacBreen, W. E. O'Grady and R. Richter, *J. Electrochem. Soc.* 1984, *131*, 1215.
- 50 [43] B. R. Scharifker, P. Zelenay and J. O. M. Bockris, *J. Electrochem. Soc.* 1987, *134*, 2714.
- 51 [44] Z. Liu, J. S. Wainright, M. H. Litt and R. F. Savinell, *Electrochim. Acta* 2006, *51*, 3914.
- 52 [45] E. Birgersson, M. Noponen and M. Vynnycky, *J. Electrochem. Soc.* 2005, *152*.
- 53
54
55
56
57
58
59
60

- 1
2
3 [46] D. Pantea, H. Darmstadt, S. Kaliaguine and C. Roy, *Appl. Surf. Sci.* 2003, 217, 181.
4 [47] W. Sun, B. A. Peppley and K. Karan, *Electrochim. Acta* 2005, 50, 3359.
5 [48] A. A. Kulikovskiy, J. Divisek and A. A. Kornyshev, *J. Electrochem. Soc.* 1999, 146, 3981.
6 [49] N. P. Siegel, M. W. Ellis, D. J. Nelson and M. R. Von Spakovsky, *J. Power Sources* 2003,
7 115, 81.
8 [50] J. Ihonen, F. Jaouen, G. Lindbergh, A. Lundblad and G. Sundholm, *J. Electrochem. Soc.*
9 2002, 149.
10 [51] F. Jaouen, G. Lindbergh and G. Sundholm, *J. Electrochem. Soc.* 2002, 149.
11 [52] K. Karan, *Electrochem. Commun.* 2007, 9, 747.
12 [53] J. M. Thomas and W. J. Thomas, *Introduction to the principles of heterogeneous*
13 *catalysis*, Academic Press, London ; New York, 1967.
14
15
16
17
18
19
20
21

22 **Page 31: [66] Formatted** ScholarOne 4/7/2010 6:21:00 AM

23 Font: 10 pt, Complex Script Font: 10 pt

24 **Page 31: [66] Formatted** ScholarOne 4/7/2010 6:21:00 AM

25 Font: 10 pt, Complex Script Font: 10 pt, Check spelling and grammar

26 **Page 31: [66] Formatted** ScholarOne 4/7/2010 6:21:00 AM

27 Font: 10 pt, Complex Script Font: 10 pt

28 **Page 31: [67] Formatted** 4/7/2010 11:20:00 AM

29 Font: 10 pt, Complex Script Font: 10 pt

30 **Page 31: [68] Formatted** ScholarOne 4/7/2010 6:21:00 AM

31 Font: 10 pt, Complex Script Font: 10 pt

32 **Page 31: [68] Formatted** ScholarOne 4/7/2010 6:21:00 AM

33 Font: 10 pt, Complex Script Font: 10 pt, Check spelling and grammar

34 **Page 31: [68] Formatted** ScholarOne 4/7/2010 6:21:00 AM

35 Font: 10 pt, Complex Script Font: 10 pt

36 **Page 31: [69] Formatted** 4/7/2010 11:20:00 AM

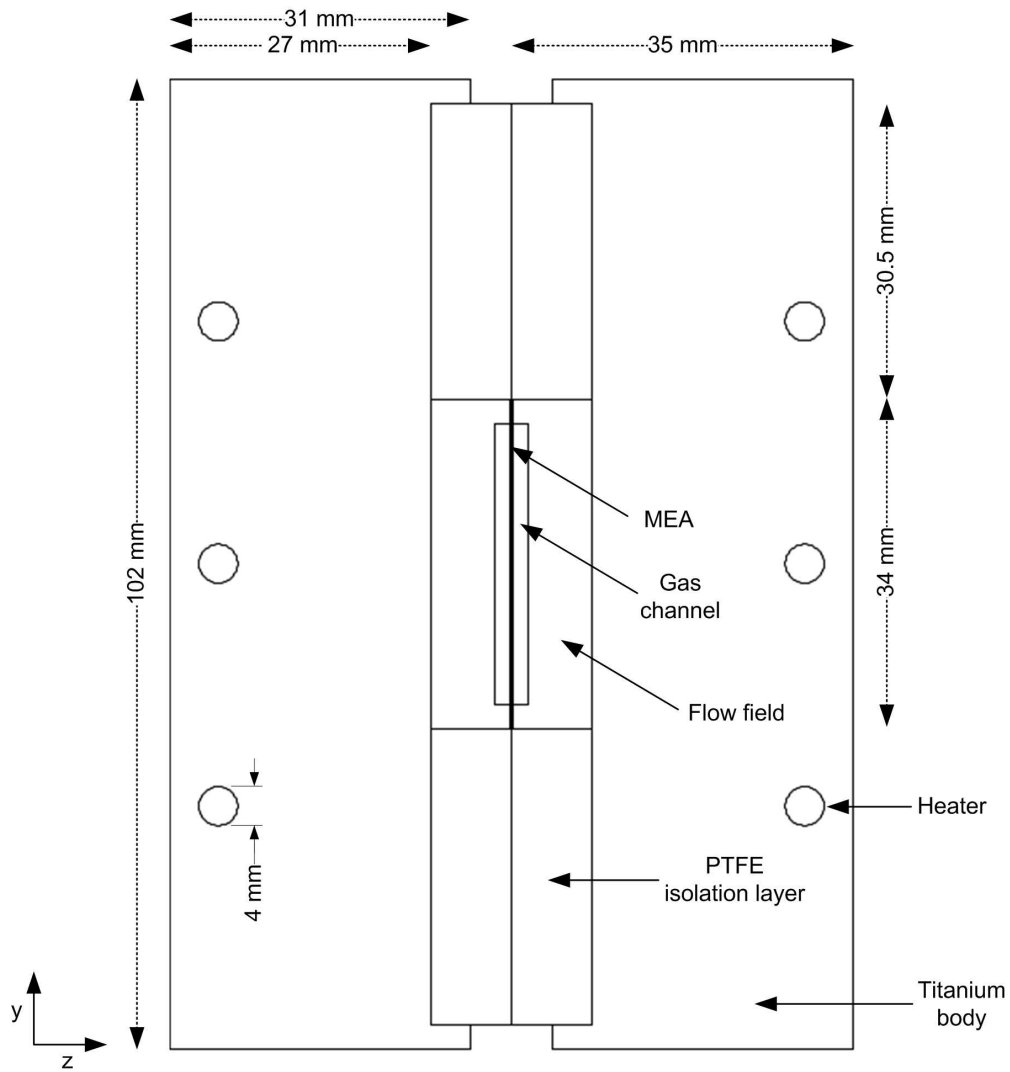
37 Font: 10 pt, Complex Script Font: 10 pt

38 **Page 31: [70] Formatted** 3/29/2010 4:31:00 PM

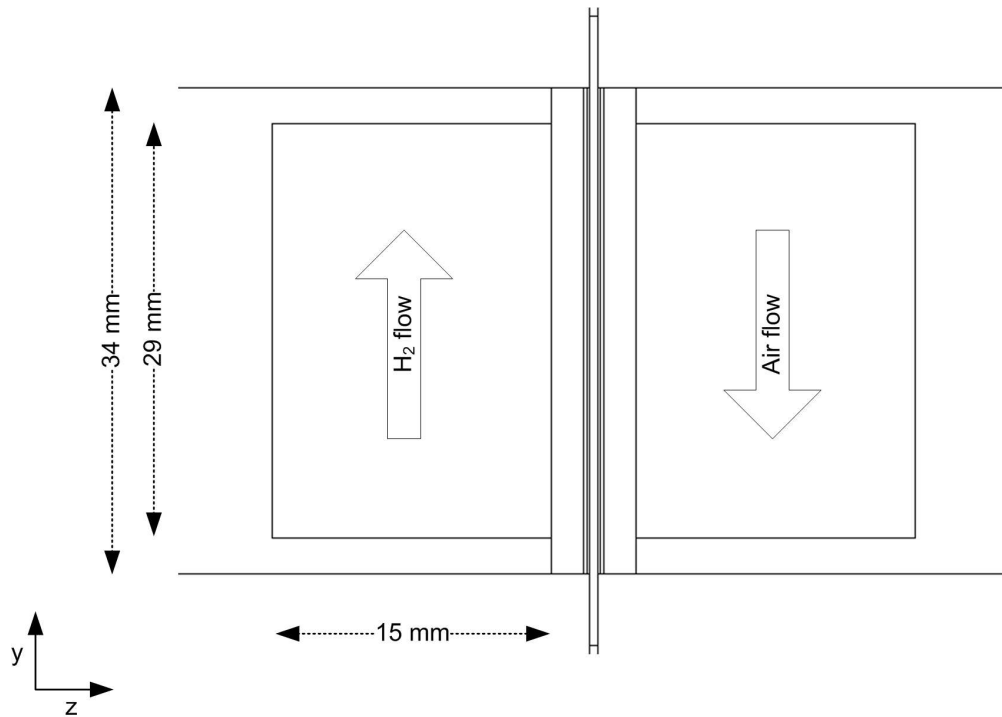
39 Font: Not Italic

40 **Page 31: [70] Formatted** 3/29/2010 4:31:00 PM

41 Subscript
42
43
44
45
46
47
48
49
50
51
52
53
54
55
56
57
58
59
60



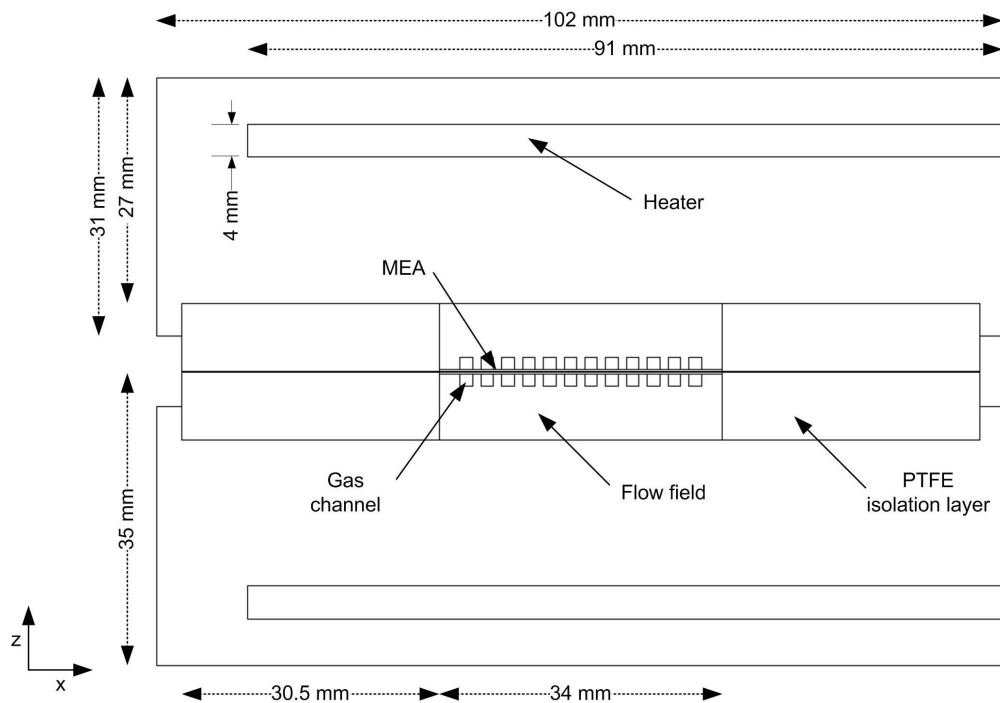
153x164mm (300 x 300 DPI)



143x102mm (300 x 300 DPI)

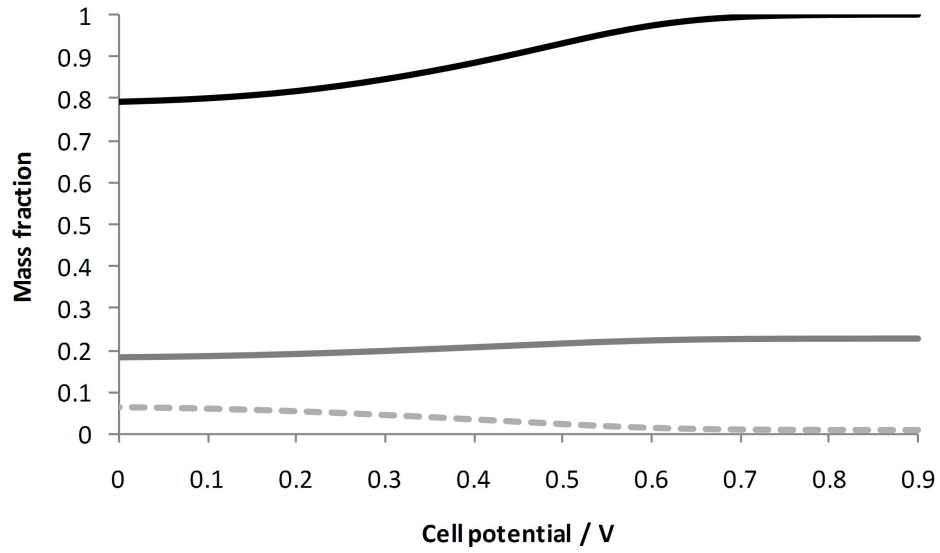
Review

1
2
3
4
5
6
7
8
9
10
11
12
13
14
15
16
17
18
19
20
21
22
23
24
25
26
27
28
29
30
31
32
33
34
35
36
37
38
39
40
41
42
43
44
45
46
47
48
49
50
51
52
53
54
55
56
57
58
59
60

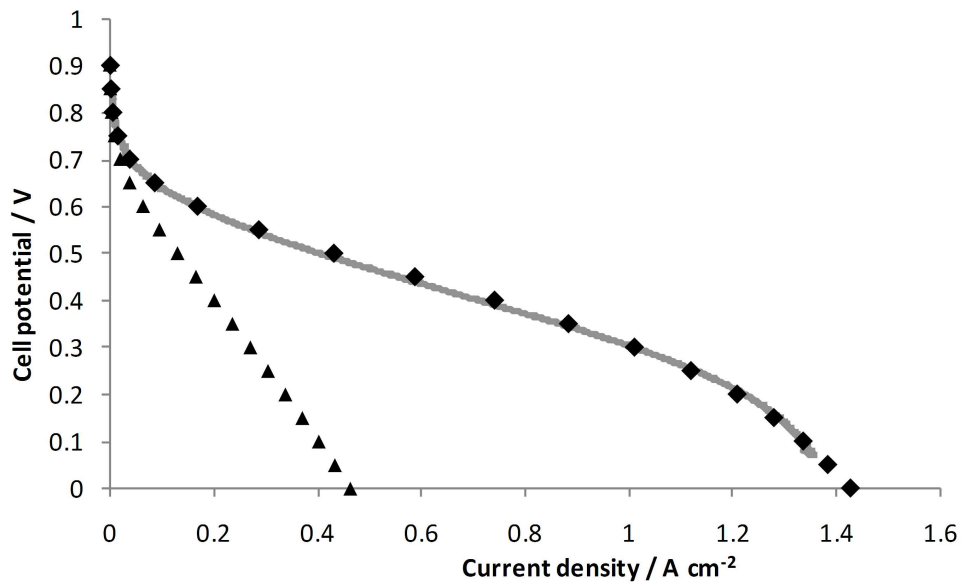


174x122mm (300 x 300 DPI)

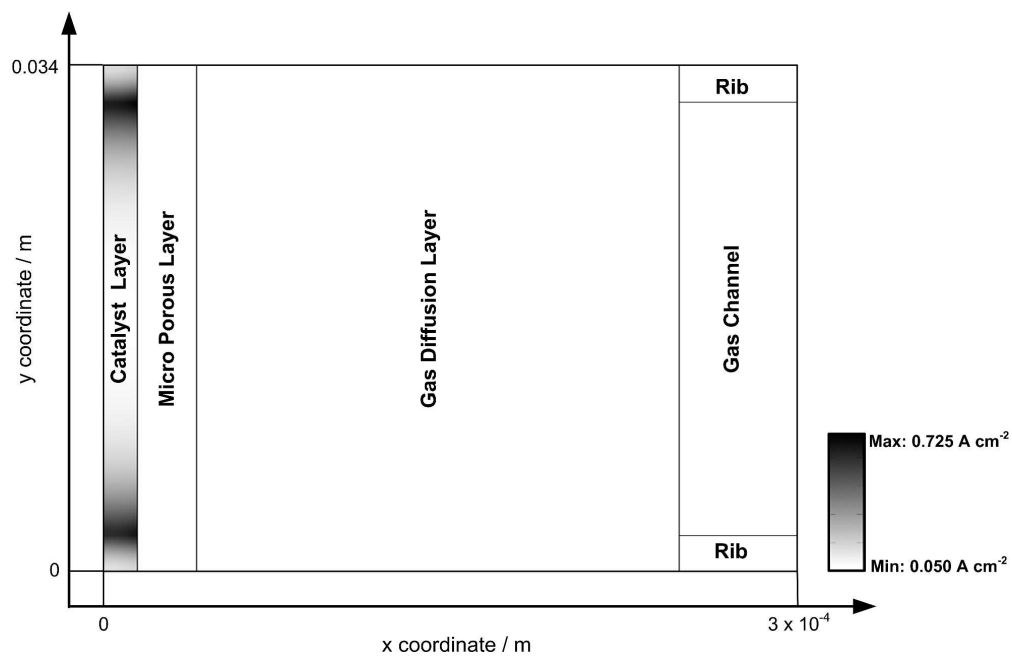
Review



120x72mm (600 x 600 DPI)



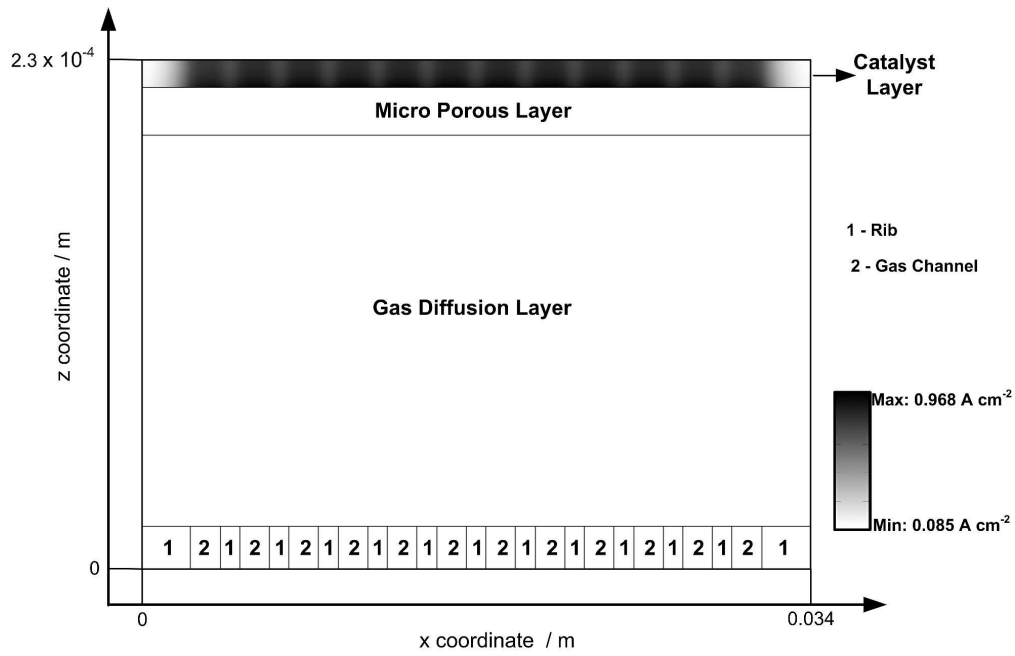
119x72mm (600 x 600 DPI)



168x108mm (600 x 600 DPI)

Review

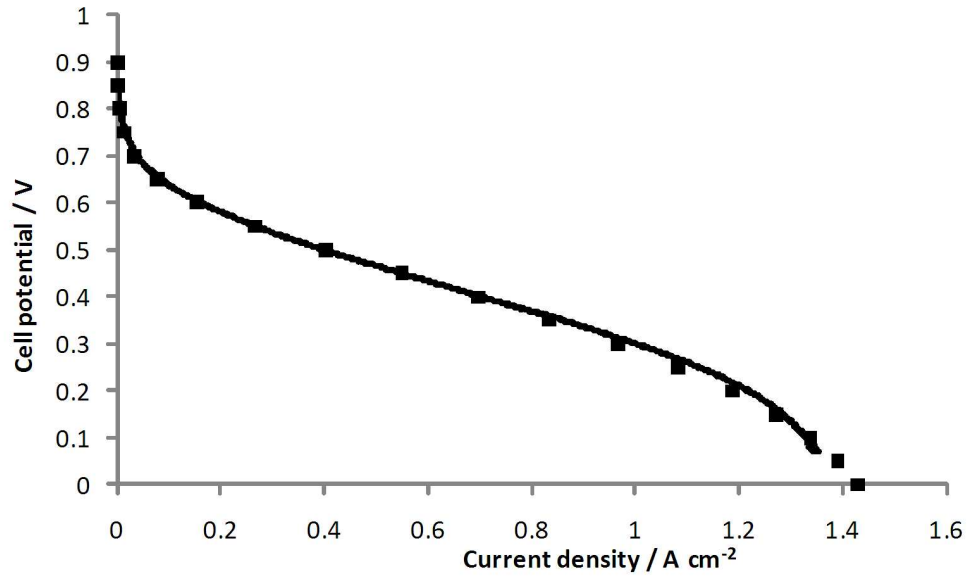
1
2
3
4
5
6
7
8
9
10
11
12
13
14
15
16
17
18
19
20
21
22
23
24
25
26
27
28
29
30
31
32
33
34
35
36
37
38
39
40
41
42
43
44
45
46
47
48
49
50
51
52
53
54
55
56
57
58
59
60



167x108mm (600 x 600 DPI)

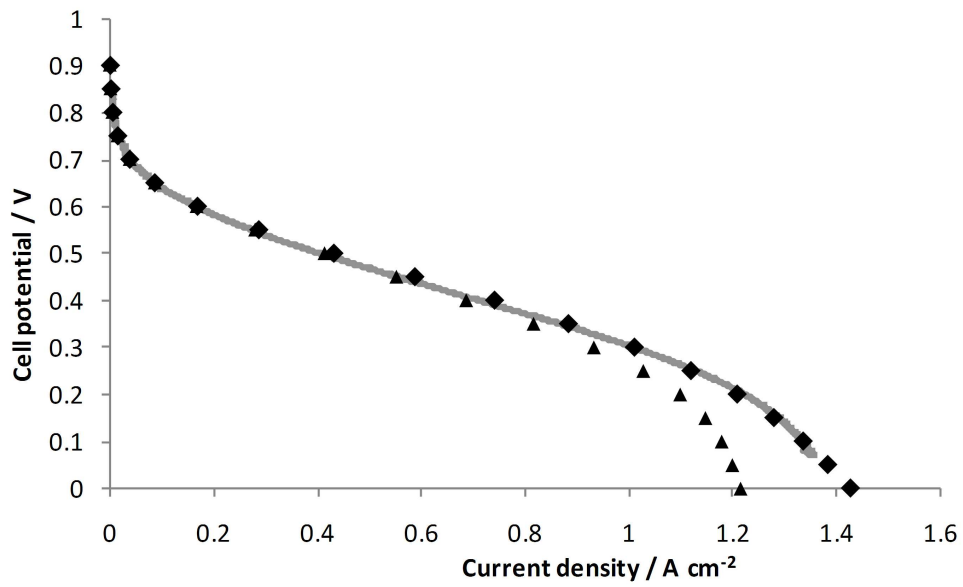
Review

1
2
3
4
5
6
7
8
9
10
11
12
13
14
15
16
17
18
19
20
21
22
23
24
25
26
27
28
29
30
31
32
33
34
35
36
37
38
39
40
41
42
43
44
45
46
47
48
49
50
51
52
53
54
55
56
57
58
59
60

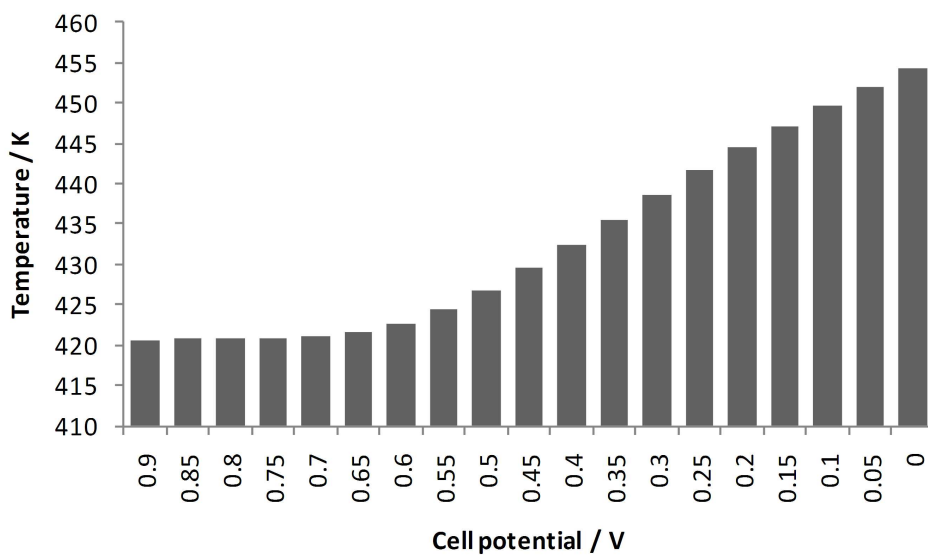


133x85mm (300 x 300 DPI)

Review



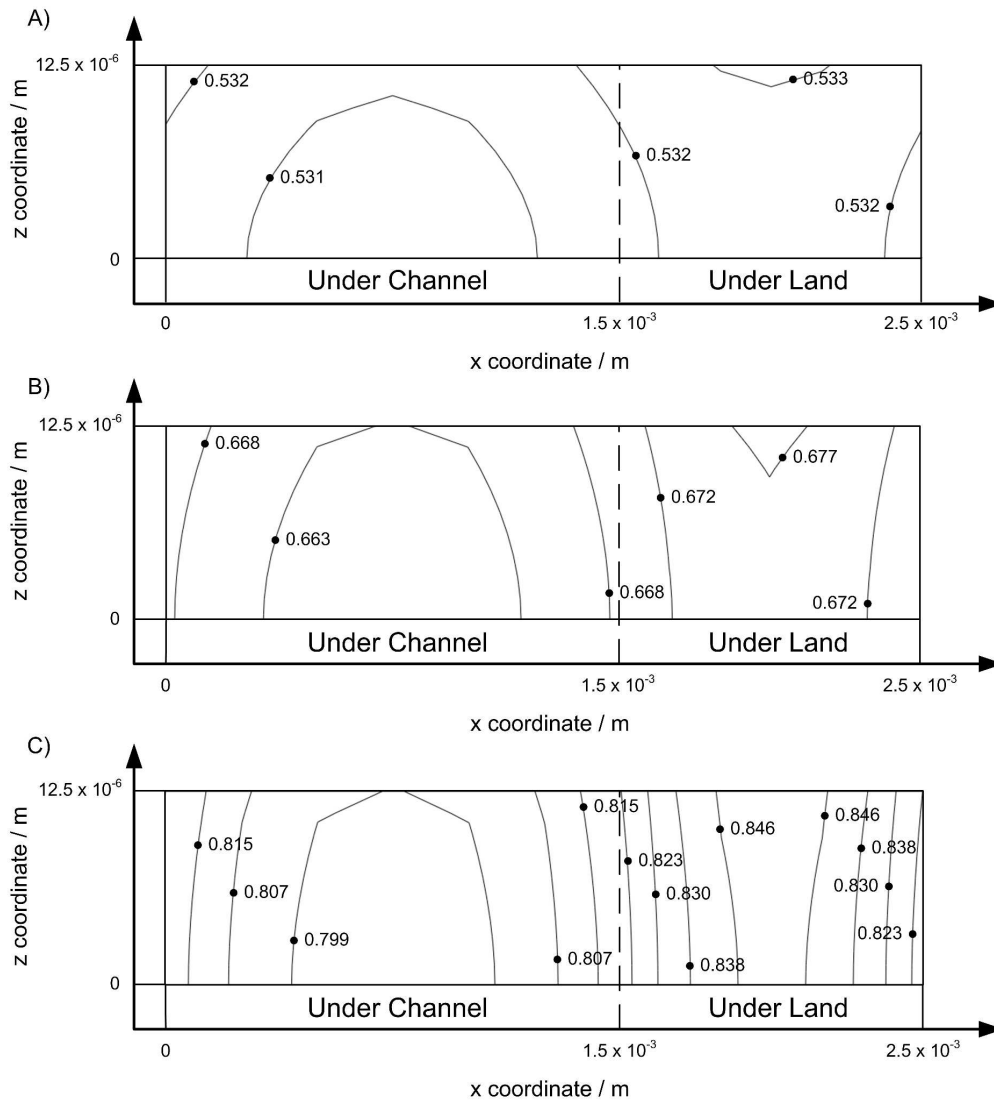
119x72mm (600 x 600 DPI)



120x72mm (600 x 600 DPI)

Review

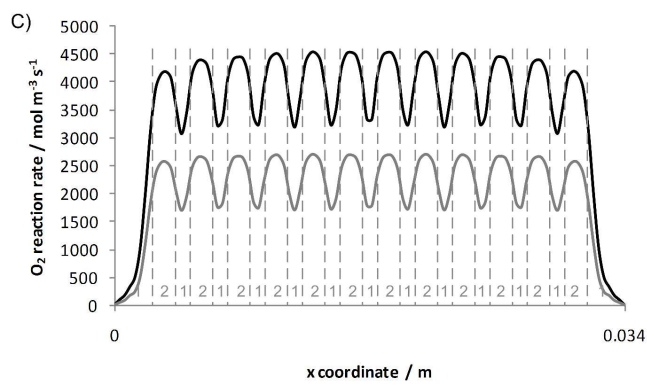
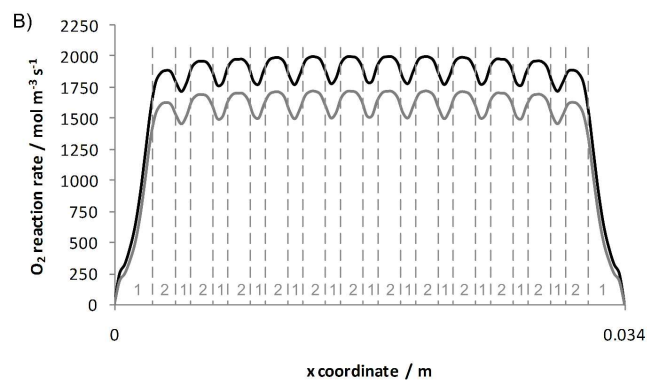
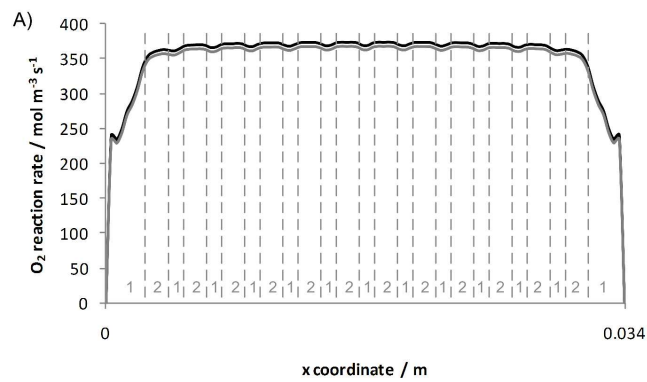
1
2
3
4
5
6
7
8
9
10
11
12
13
14
15
16
17
18
19
20
21
22
23
24
25
26
27
28
29
30
31
32
33
34
35
36
37
38
39
40
41
42
43
44
45
46
47
48
49
50
51
52
53
54
55
56
57
58
59
60



157x173mm (600 x 600 DPI)

1
2
3
4
5
6
7
8
9
10
11
12
13
14
15
16
17
18
19
20
21
22
23
24
25
26
27
28
29
30
31
32
33
34
35
36
37
38
39
40
41
42
43
44
45
46
47
48
49
50
51
52
53
54
55
56
57
58
59
60

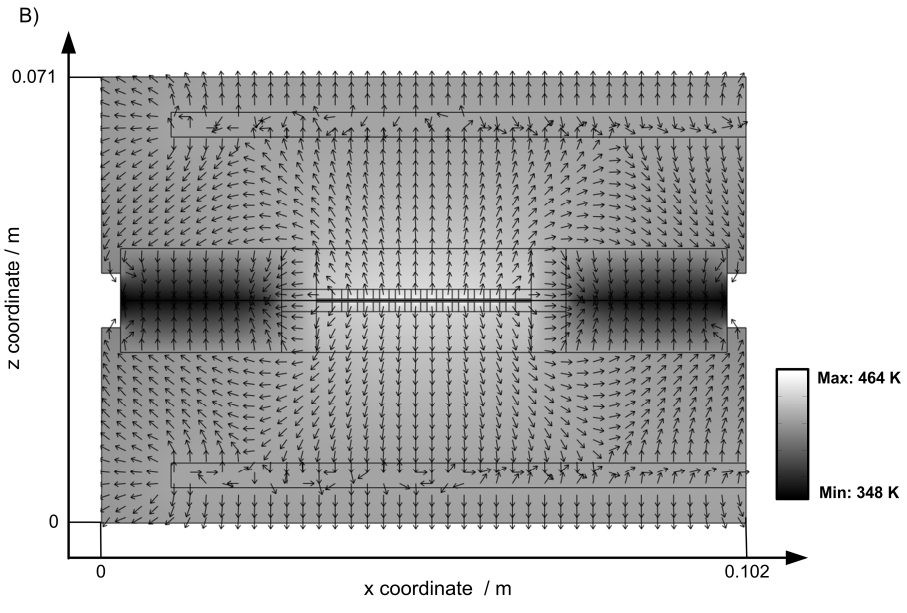
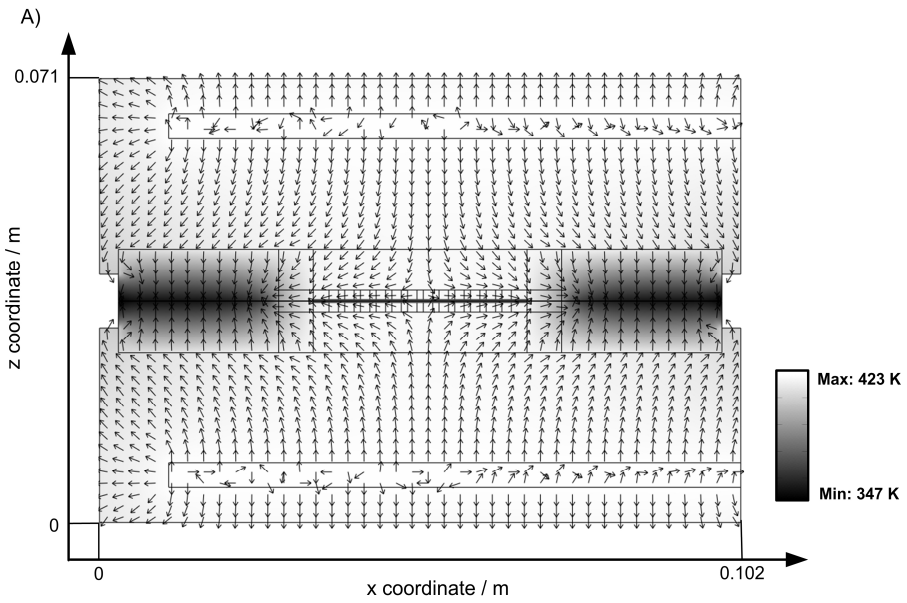
1
2
3
4
5
6
7
8
9
10
11
12
13
14
15
16
17
18
19
20
21
22
23
24
25
26
27
28
29
30
31
32
33
34
35
36
37
38
39
40
41
42
43
44
45
46
47
48
49
50
51
52
53
54
55
56
57
58
59
60



1 – Under the land 2 – Under the gas channel

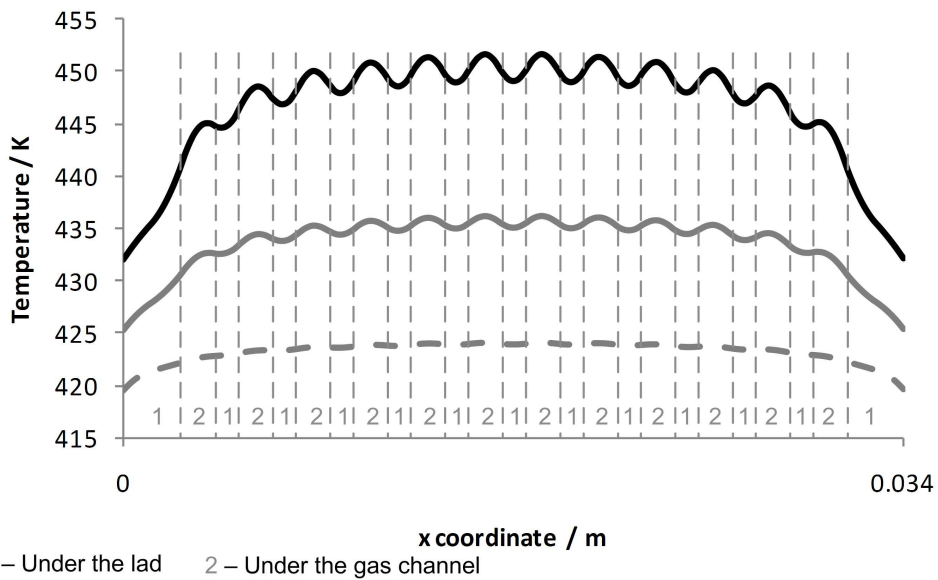
120x216mm (600 x 600 DPI)

1
2
3
4
5
6
7
8
9
10
11
12
13
14
15
16
17
18
19
20
21
22
23
24
25
26
27
28
29
30
31
32
33
34
35
36
37
38
39
40
41
42
43
44
45
46
47
48
49
50
51
52
53
54
55
56
57
58
59
60

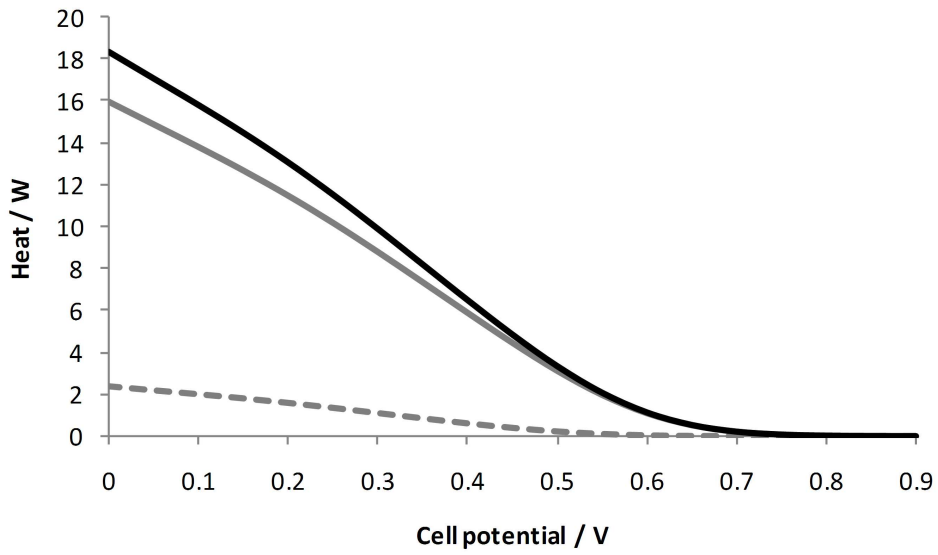


159x211mm (600 x 600 DPI)

1
2
3
4
5
6
7
8
9
10
11
12
13
14
15
16
17
18
19
20
21
22
23
24
25
26
27
28
29
30
31
32
33
34
35
36
37
38
39
40
41
42
43
44
45
46
47
48
49
50
51
52
53
54
55
56
57
58
59
60



120x72mm (600 x 600 DPI)



120x72mm (600 x 600 DPI)